Indian Journal of Geology
Vol. 72, No. 1, p. 1-29, 2000

ANALYSIS OF DEFORMATIONAL STRUCTURES ASSOCIATED WITH RIGID INCLUSIONS: AN OVERVIEW OF RECENT DEVELOPMENTS

SUSANTA KUMAR SAMANTA, NIBIR MANDAL AND CHANDAN CHAKRABORTY*
Department of Geological Sciences, Jadavpur University, Calcutta - 700032
**Geological Studies Unit, Indian Statistical Institute, Calcutta - 700035*

ABSTRACT

This paper reviews different continuum models characterizing the flow fields around rigid inclusions hosted in a ductile matrix. It can be shown that diverse types of structures that form under the influence of the heterogeneous strain around inclusions can be analyzed with the help of a single, suitable hydrodynamic theory. Jeffery's (1922) theory is found to be more general in nature, and applicable to both equant and inequant shapes of inclusions and ideal or non-ideal shear deformation of the matrix. The application of this theory, therefore, has advantages over other models, based on Lamb's theory dealing with spherical inclusions. This paper also provides a detailed discussion on existing numerical models, which are buttressed upon hydrodynamic theories, simulating the heterogeneous flow field and associated structures around inclusions. The review finally illustrates numerical simulations, highlighting the controls of physical and kinematic factors on the progressive development of some important structures associated with rigid inclusions, namely foliation drag and strain shadows around inclusions, mantle structures around porphyroclasts and inclusion trails within synkinematic, rotating porphyroblasts.

Key words : Deformation, rigid inclusions, rotation, inclusion trails.

INTRODUCTION

Rocks often contain stiff or rigid inclusions such as large mineral grains (porphyroblasts or porphyroclasts), xenoliths, pebbles etc. floating in a ductile matrix. Studies on the deformation behaviour of such rock systems have been along three principal directions: (1) The kinematics of rigid or stiff inclusions, i.e. how the floating objects change their shape or rotate bodily in the course of progressive deformation and what are the factors that control the instantaneous rate of rotation of the inclusions etc. (2) Rock systems characterized by stiff or rigid objects floating in a ductile matrix are essentially heterogeneous in nature and a variety of micro- to macro-scale structures, such as foliation drag, pressure shadow, porphyroclast tails, porphyroblast inclusion trails and intragranular fractures, develop under the influence of the heterogeneous strain field around the inclusions. The analysis of the aforesaid structures in relation to the heterogeneous flow around inclusions has gained importance in structural geology for their precise and proper application in the kinematic analysis of deformed rocks. (3) The presence of rigid inclusions in a rock also influences the bulk strength of the rock depending upon the volume fraction of inclu-

The Editorial Board has decided to bring out a review article on topics of current interest in each issue of the Journal. This is the first such article and it is on a topic which has attracted much attention in recent years from both structural geologists and metamorphic petrologists - Ed

sions, their shapes and orientations. Studies along this line have been in vogue using the mechanics of fiber composites (Cox, 1952) or viscous materials containing suspended particles (Einstein, 1911; Jeffery, 1922).

This paper exclusively deals with the second line of work and reviews the experimental and theoretical studies pertaining to the analysis of several structures associated with rigid inclusions in relation to the flow field in the neighbouring matrix.

FLOW FIELD AROUND ROTATING RIGID INCLUSIONS

Theoretical formulations

The mechanical analysis of different geological structures arising from the deformation of a rock system containing rigid inclusions within a ductile matrix hinges on characterization of three fundamental aspects: 1) rotation and shape of the inclusion, 2) the flow of the surrounding matrix and 3) the type of deformation (pure shear, simple shear or a combination of them). The theoretical formulation of the deformation pattern of such a system requires determination of the rotation rate of the inclusion and the velocity field in the surrounding matrix. Such formulations, however, also demand assumptions on the rheology of the matrix, for example whether the matrix is elastic or viscous, Newtonian or Non-Newtonian etc.

Considering elastic rheology and using plane theory of elasticity (Muskhelishvilli, 1953) several workers have analyzed the kinematics of stiff objects floating in a softer matrix and the neighboring strain field (Eshelby, 1957, 1959; Ghosh and Sengupta, 1973; Mandal and Chakraborty, 1990; Ji et al., 1997). Experimental studies, however, reveal that rocks can undergo a limited elastic strain and that too at upper crustal levels only; consequently the elastic models are unsuitable for characterizing deformation of rocks that may have undergone large ductile strain at deeper crustal levels. Application of the theories of hydrodynamics, on the other hand, appears to be more appropriate for modeling deformation behavior of rock systems containing stiff inclusions in a viscous matrix. Using Lamb's (1932) theory of spherical harmonics, Gay (1968) has modeled the deformation of floating objects within a matrix with respect to the bulk strain, for different viscosity contrasts between the object and the matrix. He derived the velocity functions as follows :

Velocity components outside the inclusion,

$$u' = \frac{1}{2}A_{-3}\rho^3 x\left(x^2 - y^2\right)/r^5 + B_{-3}\rho^5 \left[-5x\left(x^2 - y^2\right)/r^7 + 2x/r^5\right] + \dot{\bar{\varepsilon}}x$$

$$v' = \frac{1}{2}A_{-3}\rho^3 y\left(x^2 - y^2\right)/r^5 + B_{-3}\rho^5 \left[-5y\left(x^2 - y^2\right)/r^7 - 2y/r^5\right] - \dot{\bar{\varepsilon}}y$$

Velocity components inside the inclusion,

$$u = A_2\rho^{-2}\left[(5/21)xr^2 - (2/21)x\left(x^2 - y^2\right)\right] + 2B_2x$$

$$v = A_2\rho^{-2}\left[-(5/21)yr^2 - (2/21)y\left(x^2 - y^2\right)\right] - 2B_2y$$

where $r = \sqrt{x^2 + y^2}$; $\rho = b/\sqrt{1 - e^2\cos^2\alpha}$, e is the eccentricity of the elliptical object a and b are the major and minor axial dimensions of the object respectively; A, B are constants, which need to be determined by applying boundary conditions. $\dot{\bar{\varepsilon}}$ is the principal rate of natural strain in the far-field.

Gay's work reveals that the deformation within the object is essentially homogeneous, whereas the deformation outside the object is heterogeneous, as also obtained from elastic models (Eshelby, 1957, 1959). However, in Gay's mathematical formulation it is not explicit how rotating objects affect the heterogeneous flow field in the matrix, although from Lamb's theory one can also determine the velocity functions around a spherical rigid body in terms of its rotation rate by solving the famous Navier-

Stoke's equation (Oertel, 1965; Wakiya, 1956), which have been utilized to model different aspects of heterogeneous deformation around rigid objects, e.g. particle paths, strain distribution, distortion patterns of foliations (Masuda and Ando, 1988), porphyroclast tails (Bjornerud and Zhang, 1995) and inclusion trail patterns of synkinematic porphyroblasts (Masuda and Mochizuki, 1989) assuming a Newtonian rheology for the matrix.

Masuda and Ando (1988) have expressed the velocity functions outside a rigid, spherical inclusion as:

$$(u_a, v_a, w_a) = (u_{a1}, v_{a1}, w_{a1}) + (u_{a2}, v_{a2}, w_{a2})$$

The first part of the right hand side of the equation refers to the velocity components considering a general viscous flow around a fixed rigid spherical body, whereas the second part represents the velocity components arising due to the rotational motion of the rigid body. The expressions of these velocity components are as follows,

$$u_{a1} = \sum_{n=1}^{\infty}\left\{\frac{(n+1)r^{1-2n}}{n(2n+1)(2n-1)}\frac{\partial}{\partial x}\left(r^{2n+1}\chi_{-n-1}\right) - \frac{r^2}{2(2n+1)}\frac{\partial}{\partial x}\chi_{-n-1} + \frac{\partial}{\partial x}\phi_{-n-1} + \left(z\frac{\partial}{\partial y} - y\frac{\partial}{\partial z}\right)\psi_{-n-1}\right\}$$

where $r = \sqrt{x^2 + y^2 + z^2}$ and χ_n, ϕ_n and ψ_n are spherical solid harmonics of degree n.

The form of the expressions of v_{a1} and w_{a1} will be similar as above. The expression of the velocity component in the second part is:

$$u_{a2} = \sum_{n=1}^{\infty}\left\{\frac{nr^{2n+3}}{(n+1)(2n+1)(2n+3)}\frac{\partial}{\partial x}\left(\frac{\chi_n}{r^{2n+1}}\right) - \frac{r^2}{2(2n+1)}\frac{\partial}{\partial x}\chi_n + \frac{\partial}{\partial x}\phi_n + \left(z\frac{\partial}{\partial y} - y\frac{\partial}{\partial z}\right)\psi_n\right\}$$

The form of the expressions of the other two components will be similar as above.

Similarly, Bjornerud and Zhang (1995) have defined the velocity field by adding two velocity components, one associated with displacement (u_a, v_a, w_a) of material points around the rigid object and the other (u_b, v_b, w_b) with shear induced rotation of the object. The expressions of these two types of velocity components have been obtained as,

$$u_a = (3Ua/4r^3)(1 - a^2/r^2)x^2 + U(1 - 3a/4r - a^3/4r^3)$$

$$v_a = (3Ua/4r^3)(1 - a^2/r^2)xy$$

$$w_a = (3Ua/4r^3)(1 - a^2/r^2)xz$$

and

for $r > a$

$$u_b = k\omega_0 y a^3/r^3 \qquad v_b = -k\omega_0 y a^3/r^3 \qquad w_b = 0$$

for $r < a$

$$u_b = k\omega y \qquad v_b = -k\omega_0 x \qquad w_b = 0$$

where a is the object radius, r is the radial distance of the point from the object centre, U is the rate of displacement in the shear direction far away from the object and ω_0 is the rotation rate of the object. The parameter k in the equations is an index of coupling between the object and matrix, the value of which lie in the range of 0 to 1. $k = 1$ implies a non-slip condition at the object/matrix interface.

Masuda and Mizuno (1996a) and Pennacchioni et al. (2000) have further extended the analysis for rigid objects hosted in a non-Newtonian matrix. Bjornerud (1989a) formulated the heterogeneous strain field surrounding an equant rigid object following the equations of Turcotte and Schubert (1982) and numerically modeled the development of passive folds in the neighborhood of the object similar to the foliation drags obtained by Masuda and Ando (1988). The equations obtained by Bjornerud (1989) are as follows:

$$u_r = U\{-1 - a^3/(2r^3) + 3a/2r\}\cos\theta$$

$$u_\theta = U\{-1 - a^3/(4r^3) + 3a/4r\}\sin\theta \qquad (\text{for } r > a)$$

where a is the radius of the object; r and θ are polar co-ordinates centred on the sphere; u_r and u_θ are radial and tangential velocity components, re-

spectively and U is the far-field unidirectional flow velocity in the $\theta = 0$ direction. It may be noted that the above equations are applicable to fluid flow around a rigid sphere subject to the following conditions. 1) The fluid approaches a uniform velocity far away from the sphere and 2) the rigid sphere is stationary and non-rotating. Thus the velocity functions have to be modified in order to utilize them for describing the flow field around a rigid body under shear deformation.

The presence of floating objects results in heterogeneous flow in the matrix, and the heterogeneity is further augmented when the objects rotate during deformation. The nature of the heterogeneous flow field in the matrix again depends on the shape of the object as inequant objects rotate with changing angular velocity during progressive deformation in contrast to the constant angular velocity ($\gamma / 2$, γ is the bulk shear rate) executed by equant objects. The instantaneous rotation rate of an inequant object is controlled by the shape and orientation of the object at an instant and the ratio between the rates of flattening and simple shear in the general type of bulk deformation (Ghosh and Ramberg, 1976; Passchier, 1987). Consequently, the velocity fields, both inside and outside an inequant object, are much more complex than those deduced for equant objects in earlier studies. Jeffery (1922) has given an elegant mathematical treatment on the motion of ellipsoidal object embedded in a viscous medium. Jeffery's equations, determining the rate of rotation of an object in a laminar flow (equation 41), have been utilized to analyze the kinematics of rigid inclusions within a ductile rock (Ghosh and Ramberg, 1976; Passchier, 1987). From his theory one can also obtain functions for the instantaneous velocity field outside the rigid object not only for a simple shear but also for a general type of deformation (Jezek et al., 1999). Considering an ellipsoidal coordinate system, with the origin at the center of the rigid object, Jeffery obtains a solution of the Navier-Stoke's equation for viscous flow, and describes the instantaneous velocity field around the object. The velocity at a point is a function of the coordinate of the point, λ (ellipsoidal coordinate), with respect to the surface of the object, which is taken as the surface of reference ($\lambda = 0$). As the distance of the point from the surface of object becomes large, i.e. λ tends to infinity, the velocity tends to approach that of a homogeneous flow of the medium far away from the object. However, utilizing Jeffery's functions to derive the velocity field is complicated, as the functions have complex constants and parameters. Secondly, they are described with reference to the co-ordinate axes along the axial directions of the object, which themselves move with progressive deformation. Jezek et al. (1999) have circumvented these hurdles by solving the velocity functions numerically with the help of a computer software. Mandal et al. (2000) have utilized Jeffery's theory to model the heterogeneous flow field and development of related geological structures in a rock system containing rigid objects of either equant or inequant shape, under pure shear, simple shear or general type of bulk deformation. They have, however, considered the velocity functions in two dimensions, (equations 22 and 23 of Jeffery, 1922) and *analytically* derived the expressions for the constant terms in the functions by satisfying boundary conditions as given below.

Let us consider a rigid inclusion of axial dimensions a and b, hosted in an infinitely extended viscous medium, subjected to a shear flow at a rate, γ_b, with a flattening rate of ε_b, at right angles to the shear direction. A fixed reference, oxy, is set with x axis parallel to the shear direction and a moving reference frame ox'y' is tied with the axial directions of the rotating inclusion (Fig. 1). The a-axis of the inclusion at any instant makes an angle φ with the shear direction. In order to characterize the deformation of the matrix around the inclusion we need to know the velocity field in the neighbourhood of the inclusion, which can be derived by solving the famous Navier-Stoke's equations. Following Jeffery's (1922) approach these can be derived as:

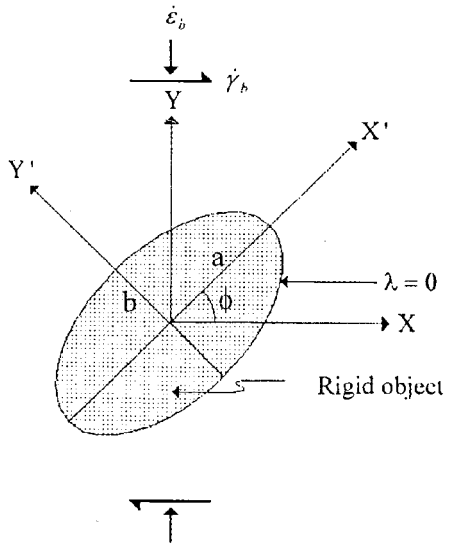

Fig. 1. Different co-ordinate systems used for derivation of the velocity functions around an inequant rigid inclusion.

$$u' = S'_{11}\left[1 - 2A(\alpha+\beta) + F\gamma\right]x' + \frac{1}{2}(S'_{12} + S'_{21})\left[2(\alpha D - \beta C) + E\gamma\right]y' + S'_{12}y'$$

$$-\frac{2\Delta x'y'}{b'^2x'^2 + a'^2y'^2}\left[\frac{1}{2}(S'_{12} + S'_{21})\left\{\frac{E + 2a'^2C + 2b'^2D}{a'^2}\right\}\right.$$

$$\left. x' + S'_{11}\left\{\frac{F - 2a'^2A + 2b'^2B}{b'^2}\right\}y'\right]$$

and

$$v' = S'_{22}\left[1 - 2B(\alpha+\beta) - F\gamma\right]y' - \frac{1}{2}(S'_{12} + S'_{21})\left[2(\alpha D - \beta C) - E\gamma\right]x' + S'_{21}x'$$

$$-\frac{2\Delta x'y'}{b'^2x'^2 + a'^2y'^2}\left[\frac{1}{2}(S'_{12} + S'_{21})\left\{\frac{E + 2a'^2C + 2b'^2D}{b'^2}\right\}\right.$$

$$\left. y' + S'_{22}\left\{\frac{F - 2a'^2A + 2b'^2)B}{a'^2}\right\}x'\right]$$

where $a' = \sqrt{a^2 + \lambda}$, $b' = \sqrt{b^2 + \lambda}$ and $\Delta = a'b'$, S'_{ij} is the instantaneous bulk strain-rate tensor with respect to axial directions of the inclusion. α, β and γ are geometric parameters, whose expressions in two-dimensions can be written as

$$\alpha = \int_{\lambda}^{\infty} \frac{d\lambda}{a'^2\Delta}, \qquad \beta = \int_{\lambda}^{\infty} \frac{d\lambda}{b'^2\Delta}, \qquad \gamma = \int_{\lambda}^{\infty} \frac{d\lambda}{a'^2b'^2\Delta}$$

The solutions of the above integrals are:

$$\alpha = \frac{2}{(a^2 - b^2)}\left[\frac{a' - b'}{a'}\right] \qquad \beta = \frac{2}{(a^2 - b^2)}\left[\frac{a' - b'}{b'}\right]$$

$$\gamma = \frac{2}{(a^2 - b^2)^2}\left[\frac{(a' - b')^2}{a'b'}\right]$$

The expressions of constants, A, B, ... in the velocity functions are:

$$A = \frac{(a+b)^2}{8}, \qquad B = -\frac{(a+b)^2}{8}, \qquad C = D = \frac{ab(a+b)^2}{4(a^2+b^2)},$$

$$E = -ab\frac{(a+b)^2}{2}, \qquad F = \frac{a^2+b^2}{4}(a+b)^2$$

Now, to find the instantaneous velocity components at a point (x, y) we first have to make the following coordinate transformation:

$$\begin{bmatrix} x' \\ y' \end{bmatrix} = \begin{bmatrix} x \\ y \end{bmatrix}\begin{bmatrix} Cos\phi & Sin\phi \\ -Sin\phi & Cos\phi \end{bmatrix}$$

where ϕ is the inclination of the a-axis to the bulk shear direction. Finally, the velocity field with respect to the fixed reference, oxy, is obtained by a reverse transformation:

$$\begin{bmatrix} u \\ v \end{bmatrix} = \begin{bmatrix} u' \\ v' \end{bmatrix}\begin{bmatrix} Cos\phi & -Sin\phi \\ Sin\phi & Cos\phi \end{bmatrix}$$

The velocity at a point (x, y) will depend on the position of the point with respect to the object boundary ($\lambda = 0$). $\lambda > 0$ indicates that the point occurs outside the object boundary, while $\lambda = 0$ and $\lambda < 0$ indicates that the points lie on the surface

and inside the object respectively. At an instant, points lying outside the object, will move with velocity components as shown above, while points either on the surface or inside the object will move with velocity components:

$$u = -\omega y \quad \text{and} \quad v = \omega x,$$

ω is the instantaneous rotation rate of the object, which is given by

$$\omega = -\frac{a^2\left(Sin^2\phi + S_r Sin2\phi\right) + b^2\left(Cos^2\phi - S_r Sin2\phi\right)}{a^2 + b^2}\dot{\gamma}_b$$

where S_r is the ratio of bulk pure shear and simple shear rates. The above equation reveals that inclusions of equant shape ($a = b$) rotate with a constant angular velocity of $\frac{\dot{\gamma}_b}{2}$ in simple shear and a combination of simple shear and pure shear.

Application of the theoretical formulations: numerical experiments

The controls of the flow field around rigid inclusions on the development of related structures are difficult to envisage directly from the velocity functions mentioned in the previous section, as their expressions are complex involving many parameters together. But, the task becomes much easier when numerical methods are applied to the expressions of the velocity functions. With the advent of computer technologies it has further become convenient to perform numerical experiments based on complex mathematical equations, which have many advantages over physical experiments. For example, in numerical experiments one can simulate deformations for high finite strains, while imposing a number of boundary conditions at a time, which is hardly possible in analog model experiments. Morcover, in physical experiments it is difficult to simulate certain structures, such as porphyroblast inclusion trails requiring an experimental set up where the analog inclusion would increase in size while rotating within the deforming matrix. In contrast, excellent inclusion trail structures can be generated with the help of numerical models. The essence of numerical modelling can be illustrated by simulating particle paths, strain distribution and foliation drag patterns around rigid inclusions as well as porphyroclast tails and porphyroblast inclusion trails using the velocity functions derived from Jeffery's theory (see following sections). The basic requirement for simulation of such features is to find the positional changes of material points at every increment of progressive deformation by using the velocity functions. This necessitates development of a simple computer programme that would compute the positional changes of all the given points, at each increment of progressive deformation, under a set of boundary conditions and would provide the final positions of the points after a finite strain so that the deformed configuration in a required finite state can be visualized. The boundary conditions are specified by several input values as required for different features, such as incremental rates of pure shear and simple shear, initial orientation of the inclusion if it is inequant, initial axial dimensions of the inclusion and its axial ratio in case of inequant shape, initial orientation of foliation markers in the matrix if there are any, incremental change in the inclusion size if it grows (e.g. synkinematic porphyroblasts) or reduces (e.g. synkinematically degenerating porphyroclasts) during progressive deformation (Table - 1).

DEFORMATION OF MATRIX AROUND RIGID INCLUSIONS

Particle paths

In order to characterize the heterogeneous flow field around rigid objects during deformation it is essential to describe the possible patterns of particle paths under varying conditions of deformation (e.g. Ramberg, 1975). In rotational deformations the presence of an equant rigid object induces concentric particle paths in the surrounding matrix. Two types of paths have been predicted - one with eye-shaped separatrix and the other with bow-tie shaped separatrix, which develop in Newtonian and

Table 1 : **An outline of computer program for numerical simulations.**

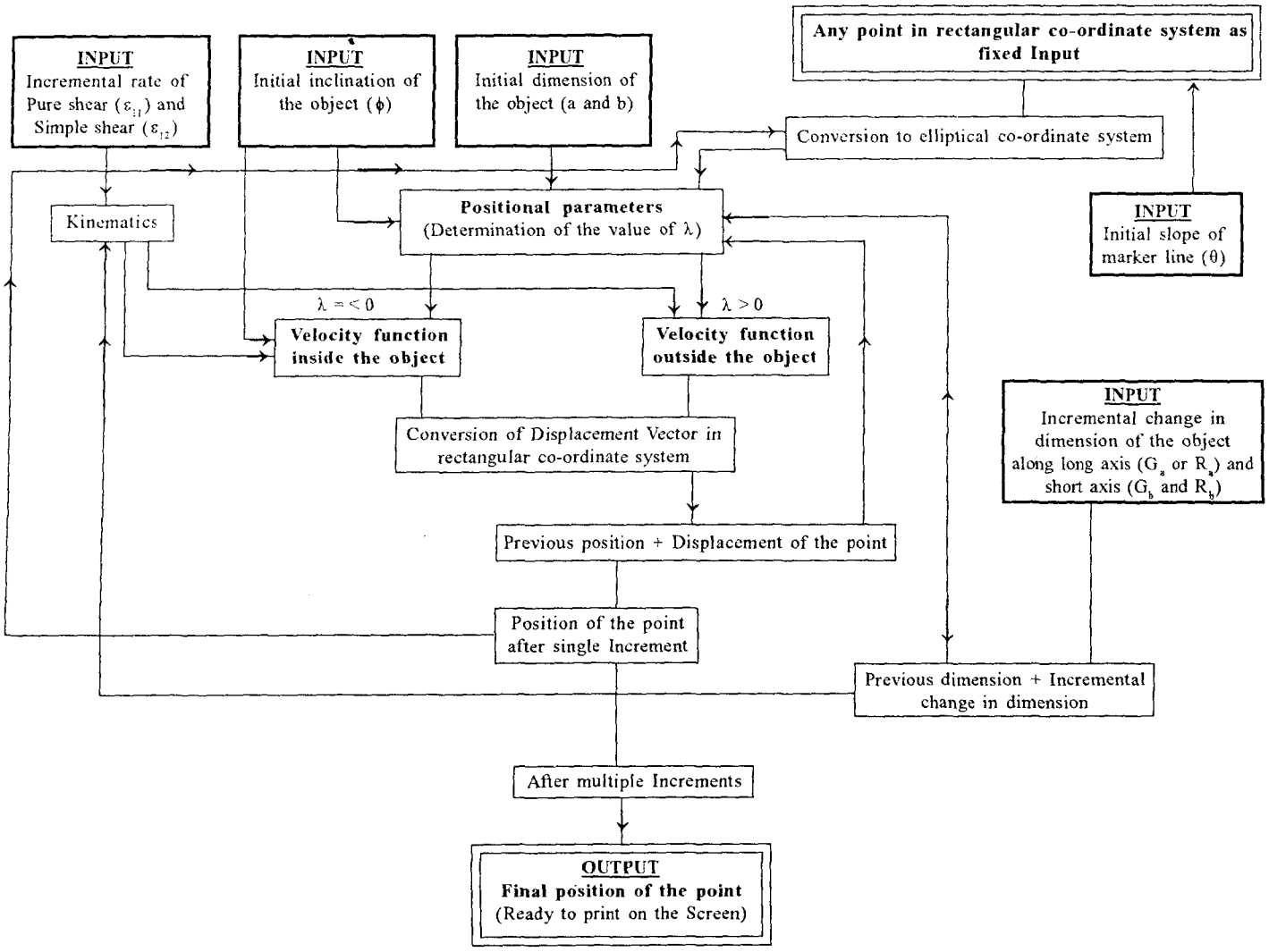

non-Newtonian matrix respectively (Fig. 2; Passchier, 1994). Later studies, however, have shown that the flow with double-bulge shaped (i.e. eye-shaped) separatrix (Masuda and Mizuno, 1996a) and bow-tie shaped separatrix (Pennacchioni et al., 2000) may develop in both the rheological varieties. It appears that in addition to matrix rheology there are other factors that could control the geometry of particle paths, such as shape of rigid inclusions ($R = a / b$) and the ratio of pure shear and simple shear rates (S_r) in the bulk deformation as pointed out by Passchier (1994).

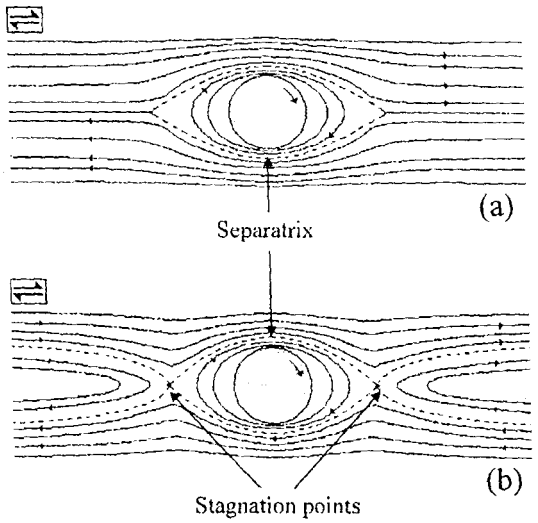

Fig. 2. Flow patterns around spherical rigid inclusions under dextral shear. (a) Particle paths with eye-shaped separatrix and (b) particle paths with bow-tie shaped separatrix (Passchier, 1994).

Influence of strain ratio (S_r) : For equant inclusions ($R = 1$) in simple shear type of deformation, the particle paths show a typical eye-shaped separatrix (Fig. 3). The separatrix has a finite dimension across its longer direction, but becomes asymptotic along the length (Fig. 3a, see also Masuda and Mizuno, 1996a). The absence of stagnation points (zero velocity) is a characteristic feature of the flow pattern around the inclusion. With introduction of pure shear component in the bulk deformation ($S_r > 0$) the separatrix becomes finite both along and across its length and two diametrically opposite stagnation points appear (Fig. 3b). With further increase in the pure shear component, particle paths in the immediate neighborhood of the object become elliptical and those away from the object are hyperbolic. The separatrix of the two types of paths assumes a bow-tie shaped geometry (Fig. 3c). The line joining the stagnation points bisects the extensional and contractional apophyses of bulk deformation (Fig. 3c). The distance between the stagnation points defines the longer dimension of the separatrix. When the pure shear component is very large ($S_r \approx 0.5$), the separatrix shrinks in size and becomes more equant, as the stagnation points moves close to the object (Fig. 3d).

To summarize, the flow pattern around an equant rigid object in simple shear is characterized by a semi-infinite eye-shaped separatrix, which in bulk deformations by a combination of simple shear and pure shear assumes a bow-tie shaped geometry with finite dimensions. The inclination of the longer dimension of finite separatrix with the bulk shear direction can be given by:

$$\theta = -\frac{1}{2}\tan^{-1}(2S_r)$$

The equation shows that the long axis of separatrix will be parallel to the shear direction when the bulk deformation is under simple shear ($S_r = 0$), as shown by Masuda and Mizuno, 1996a; Passchier, 1994.

Influence of the shape of rigid object : We have seen that inequant inclusions, unlike equant ones, rotate with changing velocity in the course of progressive deformation. As a result, the particle paths around inclusions are mutually disharmonic, and intersect one another, implying an unsteady flow around the object (Fig. 4). In case of equant objects, each particle lying between the separatrix and the surface of the object moves along a close path and reverses its movement direction twice. The points of reversals lie on the central shear plane, diametrically opposite to each other (Fig. 4a). In

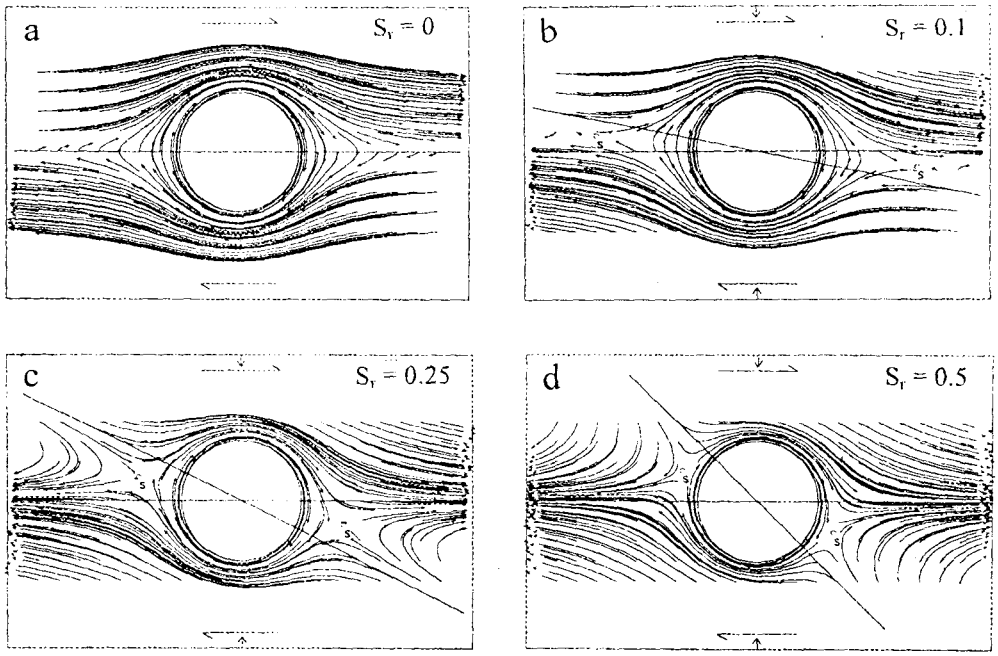

Fig. 3. Numerically simulated particle paths around equant rigid inclusions. (a) Simple shear. (b), (c) and (d) Combination of pure shear and simple shear; straight lines parallel and inclined to the shear direction are the extensional and contractional apophyses of the bulk deformation respectively. S : stagnation points in the flow around the rigid objects. S_r = ratio of pure shear and simple shear rates in the bulk deformation.

contrast, a particle in the vicinity of an inequant object reverses the movement direction several times while moving along close paths (Fig. 4b). The reversal points are generally located away from the central shear plane.

Strain shadow zones

The development of strain shadow zones around rigid mineral grains or pebbles is clearly manifested in the preferential localization of equant quartz grains on the opposite edges of rigid objects in many natural deformed rocks (Spry, 1969; Ramsay and Huber, 1987), and are so named because there the finite strain is relatively less than the far-field finite strain. The rock matrix in the strain shadow zones may remain attached to the inclusion or may be detached creating fissures between the inclusion and the matrix. These open spaces on the opposite edges of the inclusion are commonly filled with fibrous crystalline materials like quartz, calcite etc. producing structures known as pressure fringes (Ramsay and Huber, 1987). In this review we, however, deal mainly with strain shadows developing in the matrix that remain attached to the inclusion. The development of strain shadow zones can be easily demonstrated by means of physical models (Stromgard, 1973; Ildefonse and Mancktelow, 1993) as well as numerical experiments (Masuda and Ando, 1988; Masuda and Mizuno, 1996). In the following sections we shall discuss development of strain shadow zones for different strain ratios (pure shear /simple shear) and inclusion shapes by analyzing the deformations of numerous, small, initially circular markers distributed around the inclusion.

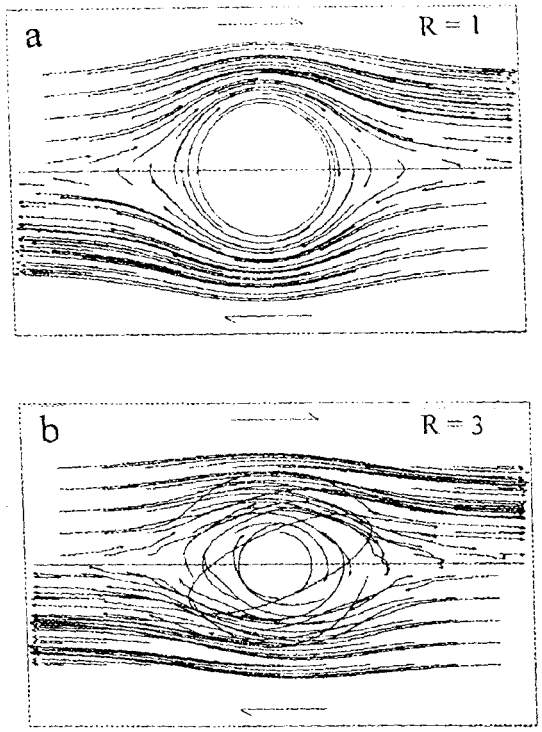

Fig. 4. Flow patterns around (a) equant and (b) inequant rigid inclusions obtained from numerical simulation. In (b) the long axis of the inclusion was initially parallel to the shear direction. R : aspect ratio of the object.

Influence of strain ratio (S_r) : In simple shear type of deformation ($S_r = 0$), strain shadow domains develop against the two extensional faces of the object describing a σ-type geometry (Fig. 5a). The zones of high strain occur near the contraction face of the object and along long bands at an angle less than 45° with the shear direction (Figs. 5a and b, see also Masuda and Ando, 1988). The low-strain zones tend to shrink as the pure shear component in the bulk deformation increases (Figs. 5 b and c), and when the deformation is entirely by pure shear no discernible strain shadow zone develops (Fig. 5d).

Strain shadow around inequant inclusions : In case of inequant inclusions the initial axial orientation of the object with respect to the shear direction (ϕ) and the axial ratio of the object (R) are additional parameters in the development of strain shadow zones. Strain shadow zones form when the long axis of the object makes an angle between 60° and 135° with the shear direction (Fig. 6). When ϕ is close to 60°, the strain shadow zone forms a narrow tail, emerging from the tip of the object (Fig. 6a). With increase in initial inclination, the shadow zone becomes wider and longer (Fig. 6b), and at ϕ= 120°, they form bands giving rise to an overall pattern similar to that of augen structures (Fig. 6c). The low-strain zones die out as the initial inclination of the object is further increases (Fig. 6d) and instead a narrow zone of strong strain concentration appears sub-parallel to the long axis of object (Fig. 6d).

For a given ϕ, with increase in axial ratio of the rigid object strain shadow zones progressively increase in length as well as change their pattern (Fig. 7). When the axial ratio is low (R = 1.5), the strain shadow zones resemble σ -type tails emerging from the nodes of the object. With increase in axial ratio, R, the zone forms wings, which finally becomes like a band surrounding the object (Fig. 7c).

Distortion patterns of passive markers

The heterogeneous flow field around rigid inclusions is often manifested in the distortion of passive markers (bedding or foliation) in the matrix. The distortion patterns of passive markers in the neighbourhood of rigid inclusions are useful in the analysis of progressive deformation as well as kinematic conditions.

Ghosh (1975), Ghosh and Ramberg (1978) have analyzed different drag patterns by considering the relative rates of rotation of the inclusion and the passive markers in the course of progressive deformation. However, there are distortion patterns that cannot be explained by these analyses. Masuda and Ando (1988) took into account the heterogeneous strain field around equant inclusions and explained diverse types of distortion patterns for different initial orientation of passive markers u-

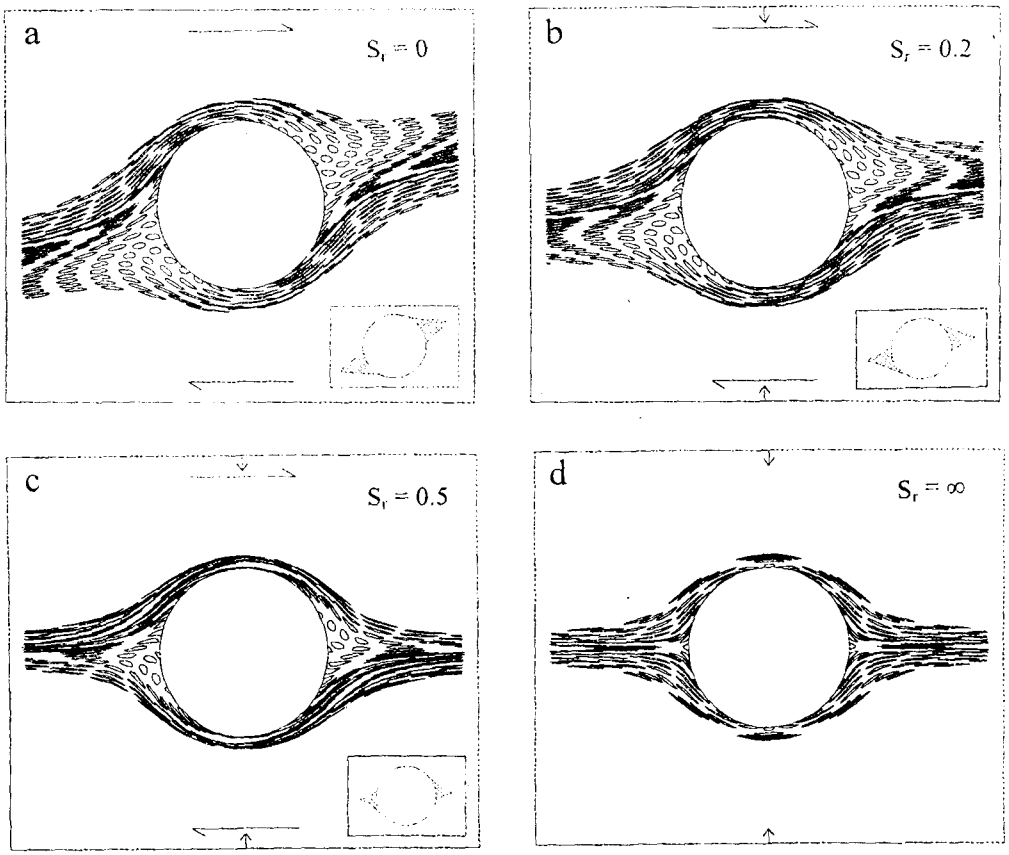

Fig. 5. Strain distributions around equant rigid inclusions in numerical models. Finite bulk shear = 4.0. Strain shadow zones (shaded) are shown in insets.

der simple shear type of bulk deformation. However, the distortion patterns would also depend on the shape and orientation of the inclusion if it is inequant and the ratio of pure shear and simple shear rates in the bulk deformation as shown in Figures 8 and 9. The different drag patterns that may form around rigid inclusions under varying conditions can be classified into four major types (Fig.10). *Type 1*: Markers form bi-convex curvatures around the object (Fig. 10a). *Type 2* : Markers are distorted in the form of typical folds on either side of the object (Fig. 10b). Depending upon the degree of relative curvature, the drag folds can again be classified into three sub types: *Type 2a, 2b* and *2c*. The first two types are characterized by larger curvatures of folds with inward convexity, and they differ from each other by the opposite sense of arrangement of folds with inward and outward curvatures. *Type 2c* has drag folds with outward convex curvatures much greater than inward convex curvatures. *Type 3* : Markers are distorted with inward convex curvatures, giving rise to geometry very similar to that of millipede structures (Bell and Rubenach, 1980). They have smooth, rounded (single-hinged) (*Type 3a*) or flat (double-hinged) (*Type 3b*) crests (Fig. 10c). *Type 4* : The drag effect of object is such that the markers are distorted in the form of overturned folds on either faces of the

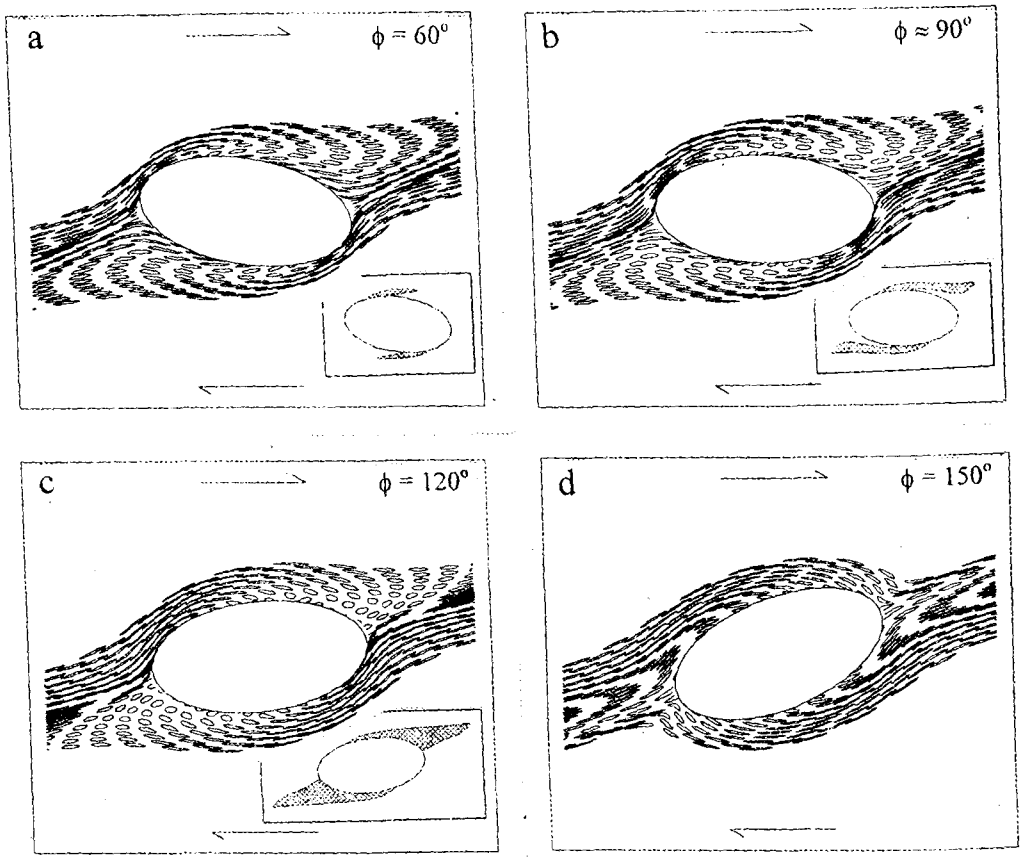

Fig. 6. Strain distributions around inequant inclusions of aspect ratio R = 2 with different initial inclinations of their long axes to the shear direction (ϕ) Finite bulk shear = 4.0. Strain shadow zones (shaded) are shown in insets.

object (Fig. 10d). This type of drag patterns has been produced in analog model experiments (Van Den Driessche and Brun, 1987). *Types 2c, 3b* and *4* develop around inequant objects under specific conditions, whereas the rest of the types are common to both equant and inequant inclusions. The nature of drag pattern of marker foliation may be useful to understand their initial orientations as well as the shear sense. For example, in case of *Type 2* drag patterns the initial orientation of the foliation is required to be parallel to the shear direction or at angles more than 90°. Again, *Type 2b* and *Type 4* drag patterns can used as shear sense indicators (Fig. 11). Table 2 summarizes the conditions at which different types of drag patterns develop.

Table 2 :

Fields of different types of drag pattern around inequant rigid objects (R = 3) in the f = q space.

	Inclination of long axis of object (f)				
	0	45	90	135	180
0	Type 3b	Type 4	Type 4	Type 2c	Type 3b
45	Type 1	Type 1	Type 4	Type 1	Type 1
90	Type 1	Type 1	Type 1	Type 1	Type 1
135	Type 2c	Type 2b	Type 3a	Type 3b	Type 2c
180	Type 3b	Type 4	Type 4	Type 2c	Type 3b

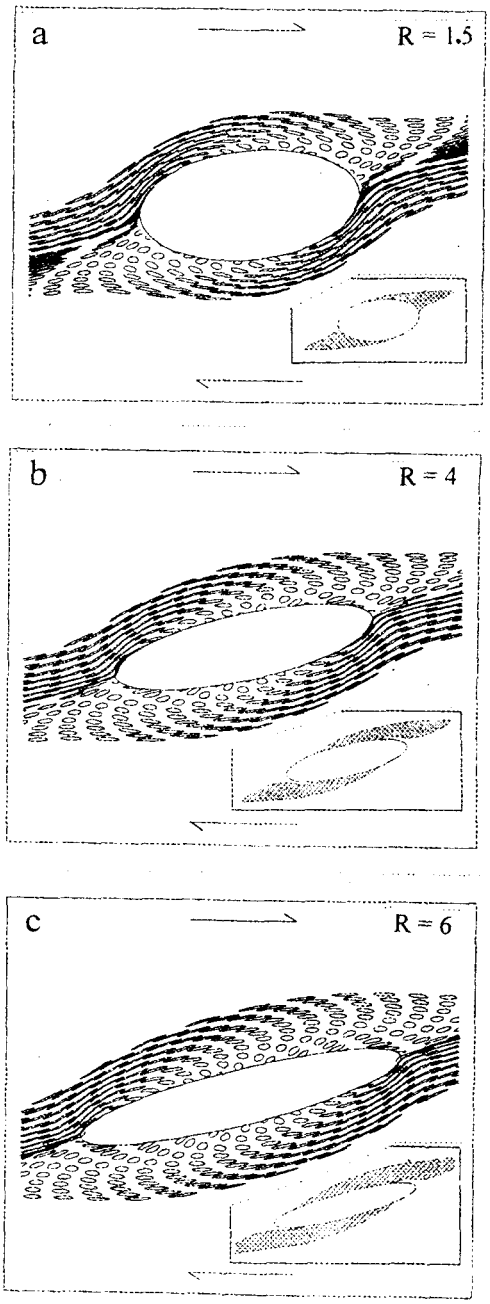

Fig. 7. Strain shadow patterns near inequant objects of increasing axial ratio R. The long axis of the objects was initially at an angle $\phi = 120°$ with the shear direcion.

MANTLE STRUCTURES AROUND PORPHYROCLASTS

The velocity functions characterizing the flow field around rigid inclusions can be utilized to study the development of mantle structures around porphyroclasts. However, in this case the porphyroclast reduces in size as a result of peripheral dynamic recrystallization in the course of progressive deformation, forming deformable mantles rimming the porphyroclast. The mantle subsequently deforms in concert with the surrounding flow field producing a spectrum of mantle structures around the porphyroclast under varying conditions of deformation. In other words, mantle structure is the deformed geometry of the mantle around the undeformed core of a porphyroclast which usually consists of tails on either side of the rigid core (Figs. 12, 13). Passchier (1994) has comprehensively classified mantled porphyroclasts into four types (θ-, δ-, ϕ- and σ- type, Fig. 12a). θ - type porphyroclasts are characterized by little or undeformed mantles without any discernible tails. σ - and δ - type porphyroclasts have mantles with prominent tails showing monoclinic arrangement. The tails on either side of the porphyroclasts lie at relatively different levels, defining stair-stepping (Fig. 12b). σ - type porphyroclasts have tails bounded by straight lines on one side and curved lines on the other side that define an internal asymmetricity. The tails in σ-type porphyroclasts do not cross the shear plane passing through the center of the porphyroclast. In contrast, δ-type porphyroclasts have tails with both boundaries curved in the same sense, and in addition, the tails cross the central shear plane. ϕ-type porphyroclasts, on the other hand have tails symmetrically disposed astride the rigid core showing an orthorhombic symmetry. σ and δ type porphyroclasts can be used as shear sense indicators by analyzing the sense of stair-stepping as shown in Figure 12b. We will see later that there may be more complex mantle structures showing combinations of the above types.

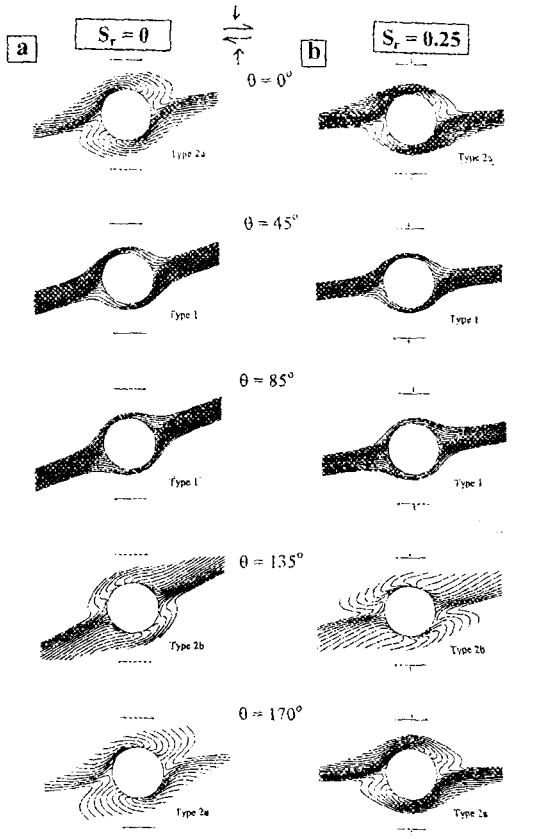

Fig. 8. Numerical simulations of the distortion patterns of passive marker lines around equant rigid inclusions. θ is the initial inclination of marker with the shear direction. (a) Simple shear. (b) Combination of pure shear and simple shear. S_r is the ratio of pure shear and simple shear rates.

Following the key publication by Passchier and Simpson (1986) mantled porphyroclast systems have increasingly gained importance in the kinematic analysis of deformed rocks, as they have been proved to be reliable shear sense indicators (Choukroune et al., 1987; Mawar, 1987; Van Den Driessche and Brun, 1987; Hooper and Hatcher, 1988; Bjornerud, 1989b; Hanmer and Passchier, 1991; Simpson and De Paor, 1993; Bjornerud and Zhang, 1994). Recent studies have revealed that the evolution of different types of mantled porphyroclasts, e.g. δ-type, σ- type etc, is itself a subject requiring a more detailed introspection (Passchier et al., 1993; Passchier, 1994; Bjornerud and Zhang, 1995; Masuda and Mizuno, 1996b). Passchier et al. (1993) and Passchier (1994) have provided genetic models for the development of mantle structures in relation to the flow perturbation around the rigid porphyroclasts. The flow perturbation that is mainly of two types, - with an eye shaped and a bow-tie shaped separatix (Fig. 2). Passchier (1994) has explained the development of the principal four types of mantle structures by considering the position of initial mantle relative to the flow separatrix.

The mantle structures of porphyroclasts have been successfully simulated in experiments with Newtonian as well as non-Newtonian matrix (Passchier and Simpson, 1986; ten Brink and Passchier, 1995; Passchier and Sokoutis, 1993). The experimental results apparently conform to the theoretical genetic models, formulated on the basis of the geometry of flow perturbations around rigid porphyroclasts (Passchier, 1994) barring some deviations (Masuda and Mizuno, 1996b). In addition, they provide a volume of information about how the mantle structures of porphyroclasts change their geometry in the course of progressive deformation to a large finite strain.

Numerical simulation (ten Brink et al., 1993; Bjornerud and Zhang, 1995; Masuda and Mizuno, 1996b) is another useful approach to study the evolution of mantled porphyroclasts. This approach has some advantages, as one can simulate a structure to high strain in a parallel-sided shear zone, while imposing a number of boundary conditions at a time. Bjornerud and Zhang (1995) have determined the stability fields of common types of mantled structures by considering synkinematic size reduction of the spherical porphyroclast at different rates and a slip or non-slip condition at the matrix-porphyroclasts interface. The model results are, however, restricted to moderate finite shear strains ($\gamma < 10$). Natural as well as experimental

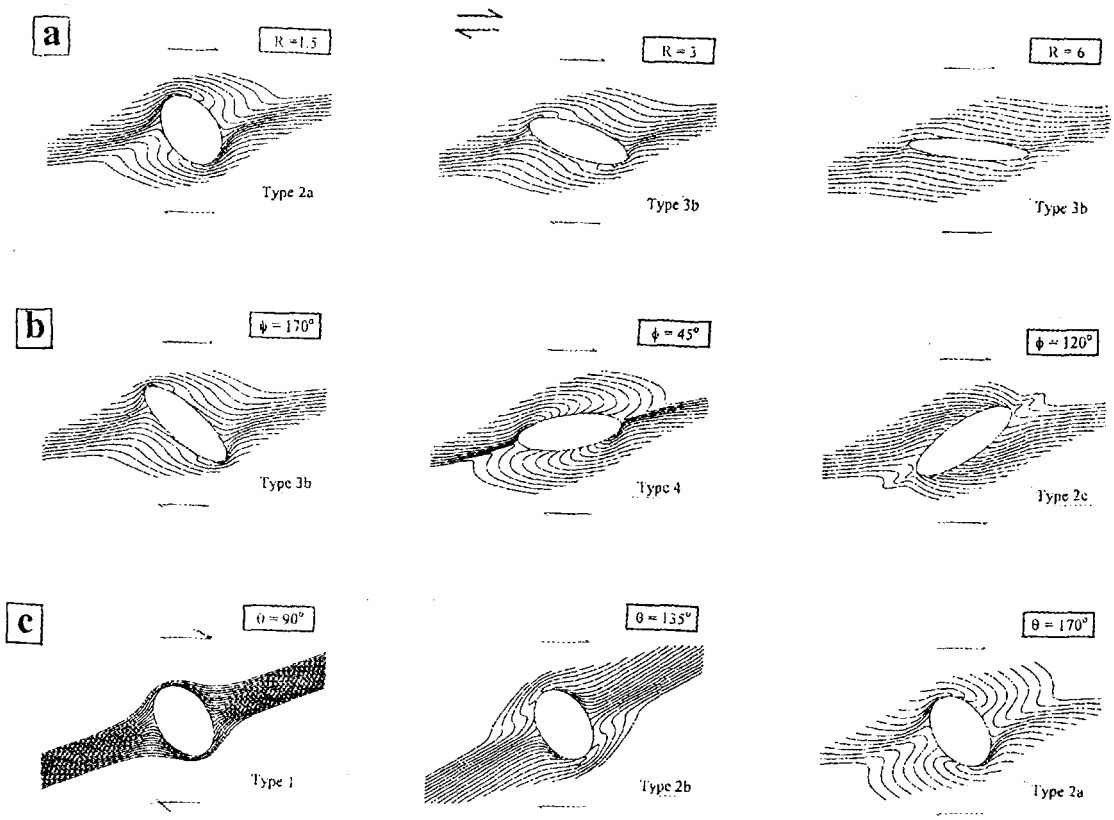

Fig. 9. Drag patterns of marker lines around inequant inclusions. (a) R was varied, keeping $\theta = 0$ and $\phi = 0$. (b) ϕ was varied, keeping $R = 3$ and $\theta = 0$. (c) θ was varied, keeping $R = 1.5$ and $\phi = 0$. In all the cases $S_r = 0$. R : axial ratio of object; ϕ : initial inclination of the long axis of object with the shear direction; θ : initial inclination of marker with the shear direction.

observations (ten Brink and Passchier, 1995) indicate that the evolution of a porphyroclast may involve a large finite strain, giving rise to additional complexities in the mantle structure. This is also evident from the numerical models of Masuda and Mizuno (1996b) where they have analyzed mantled porphyroclasts in both Newtonian and non-Newtonian matrix by varying the initial mantle width. In contrast to Bjornerud's (1995) model, their model, however, considers a fixed dimension of the object in the progressive deformation.

All these numerical models show the probable modes of development of mantle structure around equant porphyroclasts in a simple shear type of progressive bulk deformation. However, in natural mylonites porphyroclasts are often inequant in shape (Passchier and Simpson, 1986). In addition, the bulk deformation can have a shortening component across the shear zone. In detail, the shape of natural mantled porphyroclasts are thus likely to be more complex and to deviate from those so far predicted by simulations with objects of equant shape under simple shear type of progressive deformation (Passchier and Trouw, 1996). Again, the physical model experiments of Passchier and Simpson (1986) explicitly reveal that the rate of size reduction of the porphyroclast is a crucial param-

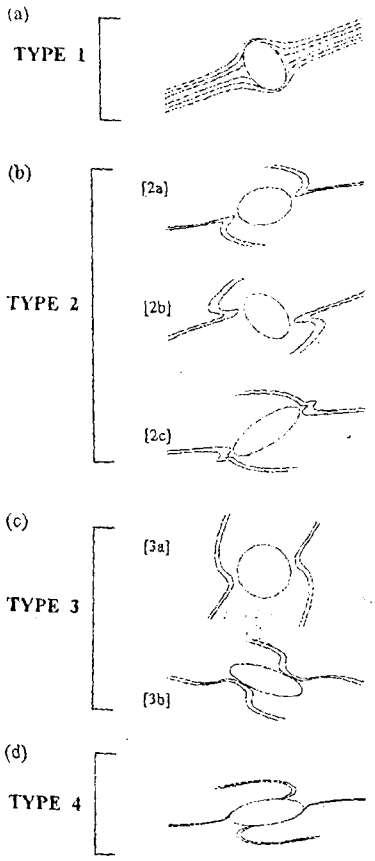

Fig. 10. Types of drag patterns obtained from numerical simulations (see text for details).

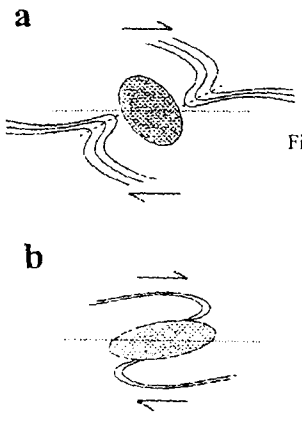

Fig. 11. Drag patterns as shear sense indicators. (a) Sidestepping of axial traces (dashed line) of inwardly convex drags. (b) Vergence of overturned drag folds on the long faces of objects with a large axial ratio.

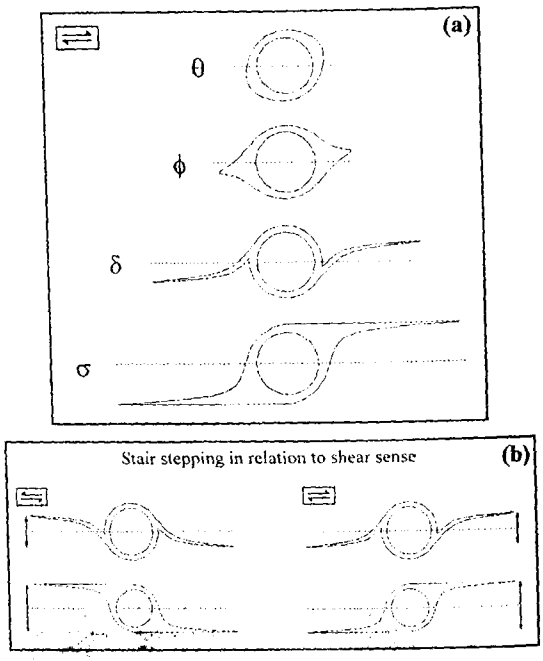

Fig. 12. (a) Types of porphyroclast systems (Passchier, 1994). (b) Relations between the sense of stair-stepping of σ and δ type porphyroclast tails and the sense of bulk shear.

eter controlling the geometry of mantle structures. Mandal et al. (2000) have presented a more generalized theoretical model in two-dimension, and shown probable patterns of mantle structure around inequant porphyroclasts in a Newtonian matrix. Their numerical simulations attempt to investigate the control of the following factors on the development of tail structures over a large finite strain: (1) the rate of size reduction of porphyroclast, (2) the ratio between pure shear and simple shear rates in the bulk deformation, and (3) the initial shape and orientation of porphyroclasts (represented by the aspect ratio a/b). This model, when applied for an equant clast and simple shear type of progressive deformation, yields results similar to those of earlier models.

In the present discussion following terms are used for the clarity of the description: *Mantle structure*- deformed geometry of the mantle around the

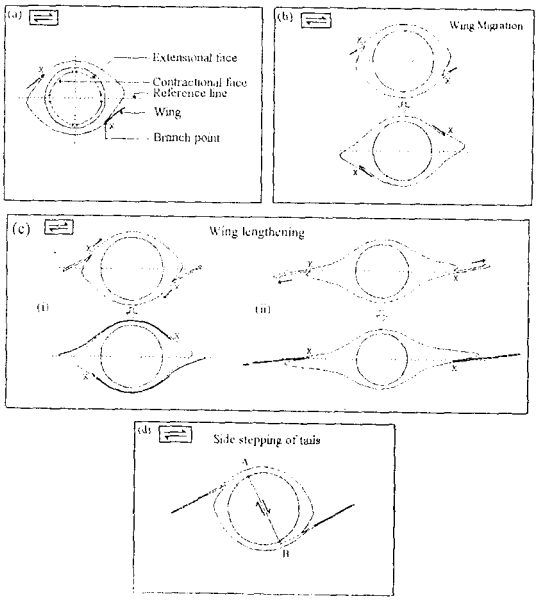

Fig. 13. Diagrammatic representation of the terminology used in the text. (a) Geometrical terms (see text for details); (b) wing migration by shifting of branch points (X); (c) wing lengthening by two modes: (i) shifting of branch points (X) without wing stretching, (ii) stretching of wings without branch point (X) shifting; (d) side stepping (A-B) in a tail structure.

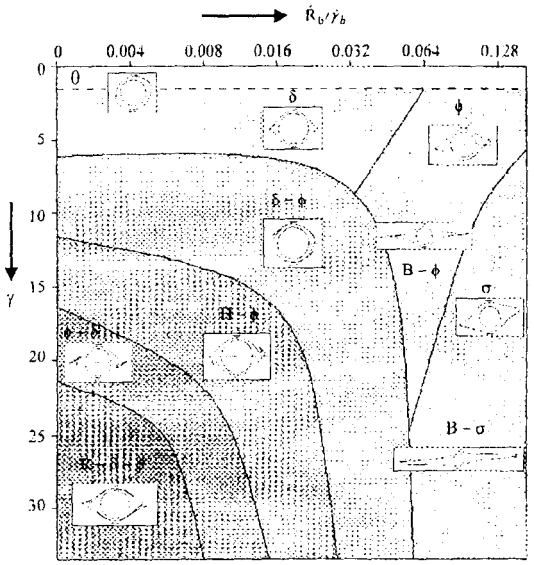

Fig. 14. Fields of different types of mantled porphyroclasts in the space of size-reduction rate (normalized to the bulk shear rate) versus finite bulk shear. δ-ϕ : ϕ tail with incipient δ wing; ϕ–δ : combination of ϕ- and δ-type geometry; H-ϕ : hooked ϕ i.e. ϕ-type tails showing hook-shaped geometry at the tip; R-δ-ϕ rolled δ–ϕ i.e. ϕ-type tails with long δ-type wings; B-ϕ : branched ϕ i.e ϕ-type tails with ϕ-type wings at the tip of the tail; B-σ : branched σ i.e. σ-type tails with short wings at the tip of the tail?

rigid core of a porphyroclast. *Tails*- the portions of deformed mantle on either side of the rigid core. *Wing*- narrow offshoots of a tail (Fig. 13a). *Branch Point*- the point from which a wing offshoots from the tail. *Wing migration*- the bodily migration of a wing along with the branch point (Fig. 13b). *Wing lengthening*- the increase in length of a wing, which occurs in two modes- (i) shifting of the branch point without wing stretching, (ii) wing stretching without branch point shifting (Fig. 13c). *Contractional face and extensional face*- portions of the object, at any instant, facing the contractional and extensional fields respectively (Fig. 13a). *Side-stepping*- refers to the lateral offset of the tails as one moves from one side of the porphyroclast to the other (Fig. 13d).

Numerical models of Mandal et al. (2000) indicate that δ-, ϕ- and finally σ- type mantle structures (Passchier, 1994) develop as the rate of clast-size reduction increases (Fig. 14). These results qualitatively conform to the model of Bjornerud and Zhang (1995) that shows the development of σ-type objects at a high rate of recrystallization. Similar results were also obtained from analog model experiments (Passchier and Simpson, 1986). For a given rate of clast-size reduction the mantle geometry changes with increasing finite shear strain during progressive deformation (Fig. 15). The stability fields of the principal mantle types have been delimited in the space of finite strain versus recrystallization rate from physical and numerical model experiments (Passchier and Simpson, 1986; Bjornerud and Zhang, 1995). These studies are, however, restricted to moderate finite strains ($\gamma \leq 10$). The simulations of Mandal et al. (2000) and Masuda and Mizuno (1996b) show development

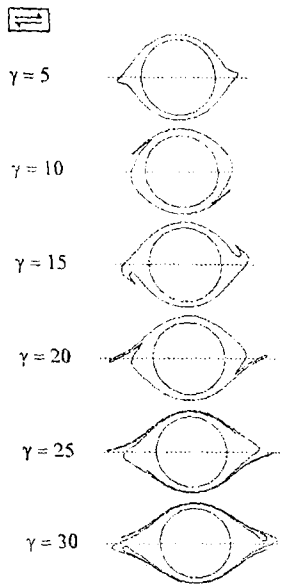

Fig. 15. Progressive development of mantle structures around equant porphyroclasts in dextral shear. Rate of size reduction (R) = 0.125.

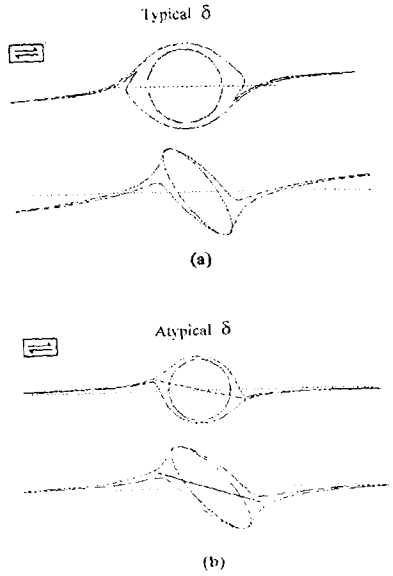

Fig. 16. (a) Typical and (b) atypical δ - type mantle structures.

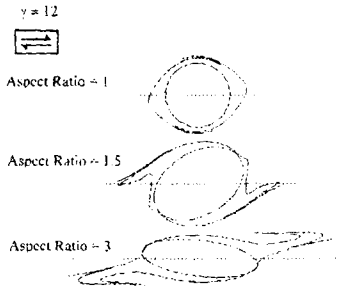

Fig. 17. Control of the shape of porphyroclasts on their mantle structures. Rate of size reduction (R) = 0.125.

of complex, but definite patterns over larger finite strains as shown in a broader field diagram (Fig. 15).

It has also been revealed that typical δ - type tails that cross the reference plane and show stair-stepping generally develop for moderate rates of clast-size reduction (0.25 - 0.5) (Fig. 16a). When the rate of clast-size reduction is lower, the mantle structure looks like incipient δ -type tails that do not cross the reference plane, which at lower values of kinematical vorticity number (i.e. higher S_r) appear as δ objects without stair-stepping but show side-stepping as defined in Fig.13 (Fig. 16b, see also Passchier et al., 1993).

For the same kinematic and physical conditions, porphyroclasts of different initial shapes develop different patterns in their mantles (Fig. 17). At a low finite strain, elongate objects with larger aspect ratio have more complex multi-winged tail patterns in comparison to those of equant objects, except at higher values of clast-size reduction rate. In natural mylonites the former may be mistaken to represent high finite shear. Such a qualitative assessment of finite strain from mantle structures may thus be erroneous unless other factors are taken into account. At higher values of S_r inequant objects also show development of δ -like tails that do not cross the central reference plane and appear as non-stair stepped δ-tails of Passchier et al. (1996). However, the mantle structure shows side-stepping (Fig. 16).

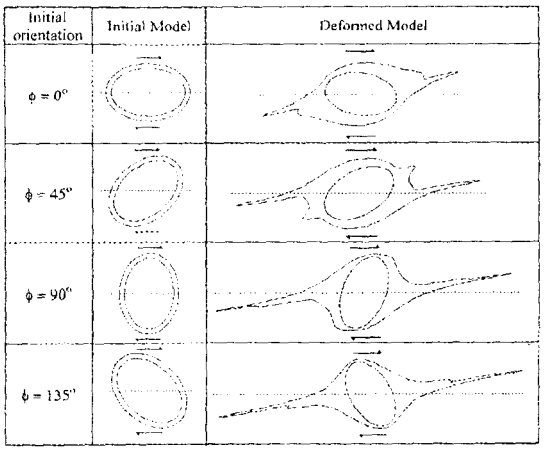

Fig. 18. Variation in the mantle geometry of inequant porphyroclasts (aspect ratio 1.5) with their initial orientation (ϕ). Finite bulk shear (γ) in all models was 7.5. Rate of size reduction (R) = 0.125.

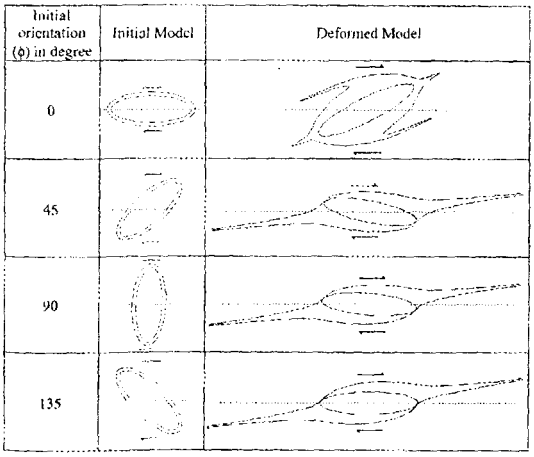

Fig. 19. Variation in the mantle geometry of very elongate porphyroclasts (aspect ratio 3) with their initial orientation (ϕ). Finite bulk shear (γ) in all models was 7.5. Rate of size reduction (R) = 0.125.

Mandal et al. (2000) performed several numerical experiments in order to study the effects of orientation of inequant porphyroclasts on the mantle geometry. In simple shear type of progressive deformation ($S_r = 0$) porphyroclasts of aspect ratio 1.5 develop δ-type mantle geometry when their long axis is initially parallel to the shear direction (Fig. 18). With increase in the initial inclination ($\phi > 20°$) the mantle tends to have a composite structure showing δ-type wings, which becomes dominant, giving rise to a δ -type overall geometry of the mantle at $\phi = 80°$. A similar transformation from σ-type to δ -type mantle geometry with change in porphyroclast orientation has been demonstrated from kinematic models (Simpson and De Paor, 1993). With further increase in the inclination ($\phi > 110°$) the mantle becomes symmetrical, forming a ϕ-type geometry.

For a given finite bulk shear, the variation of mantle geometry versus initial orientation of porphyroclast, as noticed in the above numerical examples, is different when the porphyroclast has a different initial aspect ratio. Experiments with initial aspect ratio 3 yield a contrasting result (Fig. 19). Porphyroclasts with initial orientation parallel to the shear plane develop δ-type mantle geometry and those with initial orientation perpendicular to the shear plane form σ-type mantle geometry.

Different sets of experiments were run by Mandal et al. (2000) by varying the initial orientation of porphyroclast under different values of the ratio of pure shear and simple shear rates (S_r) or kinematic vorticity number (W_k) with constant initial aspect ratio ($a/b = 2$). The experimental results are shown synoptically in Fig. 20. The mantle pattern, irrespective of initial orientation of porphyroclast, tends to assume a simpler δ -like geometry without stair-stepping at a large value of S_r or a low value of W_k. However, the S_r-value at which porphyroclasts show such a simple pattern depends on the initial orientation (ϕ) of the porphyroclast. When $\phi = 0$, the pattern develops at $S_r = 0.50$, which forms at $S_r = 0.25$, when the initial orientation ϕ is 90°.

To summarize: (1) at a low finite strain, equant objects develop simple δ - type tails, which is replaced by ϕ - type, as the rate of clast-size reduc-

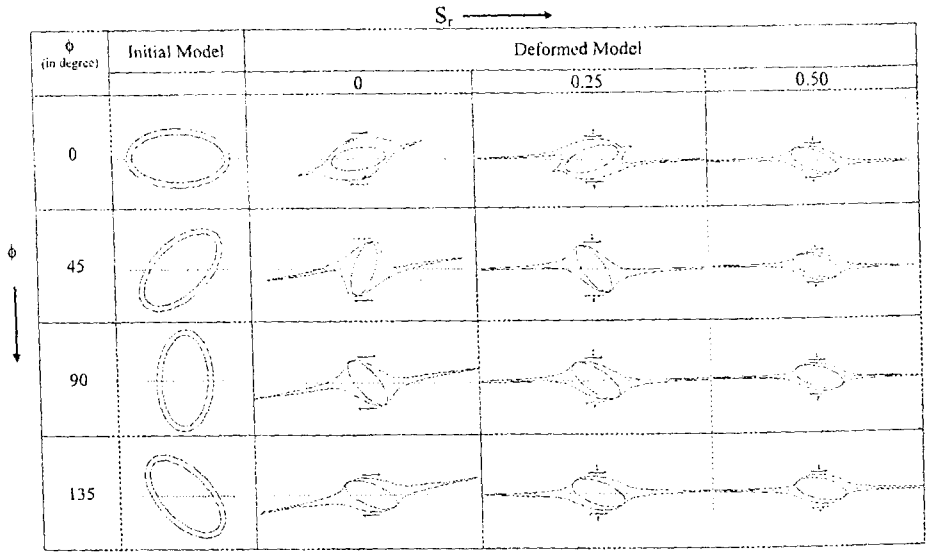

Fig. 20. Distribution of mantle patterns of inequant porphyroclasts in ϕ versus S_r space, where ϕ is the initial inclination of porphyroclast with the shear plane and S_r is the ratio of pure and simple shear rates in the bulk deformation. Rate of size reduction (R) = 0.125.

tion is increased. σ-type tails form at a high rate of clast-size reduction and a high finite strain. (2) With an increase in finite shear strain, the tails tend to have successive generations of wings forming complex mantle structures except for a very high rate of clast-size reduction. (3) Elongate objects may develop composite tail patterns consisting of multiple wings, even at low finite strains and the mantle structures become increasingly complex with increase in aspect ratio. (4) In case of inequant porphyroclast the mantle structures depend on the initial orientation of the porphyroclast. (5) For a given finite shear, decrease in the vorticity of bulk deformation leads to development of simpler mantle structures and vice-versa. (6) Porphyroclast systems have been utilized as shear sense indicators by considering the sense of stair-stepping in the mantle structures (Passchier and Trouw, 1996). However, there are mantle structures where the tails do not show stair-stepping (Fig. 16). In such cases shear sense can be determined from the side-stepping of the tails. Again, the rotation of an equant object takes place with a uniform angular velocity, while an inequant object rotates with a changing velocity. In the latter case the object may even rotate with a sense opposite to the shear sense where a flattening component acts across the shear zone (Passchier, 1987). An obvious doubt then arises on the usage of tail patterns of inequant porphyroclasts as shear sense indicators. However, the numerical models reveal that inequant objects develop more complex patterns containing multiple wings showing sense of side-stepping synthetic to the bulk shear sense. Inequant objects with multiwinged mantles can thus be reliably used for the determination of shear sense.

Kinematics of mantle deformation

Numerical experiments, described in the earlier sections reveal that the development of mantle structures involves some specific kinematics of their tails or wings, which in turn govern the final geometry of the mantle structure. This section presents a genetic basis for different mantled porphyroclast systems by considering the following three modes of mantle deformation. *Mode 1* : the mantle devel-

opment involves dominantly wing migration (Fig. 13); the wings move bodily with the rotating porphyroclast without any shortening or lengthening during migration. *Mode 2*: The mantle development is associated with wing lengthening (Fig. 13), that takes place either by branch point shifting (*Mode 2a*) or by wing stretching (Fig. 13) without branch point shifting (*Mode 2b*). *Mode 3*: The tail structures lengthen in the instantaneous extension quadrant along with the branch points.

Each mode of mantle development gives rise to a particular type of mantle structure. In *Mode 1* the wings show incipient δ-like geometry, which bodily migrate and coalesce with ϕ-type tails in the instantaneous extension quadrant, forming a hooked $\delta-\phi$ geometry at a large finite strain (Fig. 14). In *Mode 2a*, the wings grow in length, but never cross the central reference plane. The mantle therefore does not assume a typical δ-type geometry, as defined by Passchier and Simpson (1986), but forms atypical δ-type structures, which transform into a rolled $\delta-\phi$ composite geometry at a large finite strain (Fig. 15). *Mode 2b* mantle development is characterized by wing stretching, maintaining the branch points at fixed positions. The wings therefore can cross the central reference line, forming a typical δ-type geometry (Fig. 16). *Mode* 3 involves stretching of the tail structure as a whole, where the offshoots also experience stretching along with their branch points in the bulk extension direction. This mode of mantle development results in the formation of ϕ-type overall geometry.

Numerical model experiments run at different clast-size reduction rates indicate that the mode of mantle development is controlled by the size reduction rate of the porphyroclast. Low rates of size reduction favour *Mode 1* mantle development. As the mantle grows in thickness slowly, it experiences a strong drag effect induced by the rotating rigid core. The wings in them therefore migrate bodily, similar to material particles describing close paths around rigid objects (Fig. 3). With increase in size-reduction rate, *Mode 1* is replaced by *Mode 2a*. In *Mode 2a*, the mantle boundary is folded by branch point shifting, forming wings. As the porphyroclast shrinks at a faster rate, the drag influence of the rotating rigid core onto the wings decreases and thereby does not result in overall movement of the wing. The wing migration in concert with the rotating rigid core is countered by wing stretching in the bulk extension direction. At a critical balance of these two tendencies the wings do not move bodily either in the shear or extension directions. With further increase in size-reduction rate, the drag of the rigid core onto the mantle boundary becomes weak and the processes of branch point shifting due to the drag effect is therefore suppressed, whereas the wing stretching in the extension direction gets dominance. Under this condition *Mode 2b* becomes the more dominant mode in the mantle development, forming typical δ-type structures. At higher size-reduction rates the mantle grows in size suffering relatively less drag by the rotating porphyroclast. Consequently, *Mode 2* is replaced by *Mode 3*, in which wing stretching is much more important than branch point shifting, giving rise to a ϕ-type overall geometry of the mantle. In *Mode 3*, σ-type mantle structures form when the drag effect onto the mantle boundary is very little or absent.

INCLUSION TRAILS WITHIN PORPHYROBLASTS

Inclusion trails are a typical feature of many natural synkinematic porphyroblasts, which commonly record minute details of deformation history. Consequently, the study of porphyroblast systems has been in vogue over several decades (Rast, 1958; Zwart, 1960; Spry, 1963; Rosenfeld, 1970; Schoneveld, 1977; Powell and Vernon, 1979; Bell and Rubenach, 1980; Bell, 1985; Bell and Johnson, 1989; Passchier et al., 1992; Passchier and Speck, 1994; Johnson and Bell, 1996; Johnson and Moore, 1996).

Curved or spiral trails may result due to rotation of porphyroblasts as they grow over a pre-existing, passive foliation during a single phase of

deformation and metamorphism (Ghosh and Ramberg, 1978; Mandal and Banerjee, 1987; Masuda and Mochizuki, 1989; Bjornerud and Zhang, 1994; Beam, 1996). On the other hand, curved trails may also form within non-rotating, stationary porphyroblasts as they grow over and include variably oriented, successive generations of overprinting crenulation cleavages during multiple phases of deformation and metamorphism (Bell, 1985; Bell et al., 1992 a, b; Bell and Hickey, 1997; Bell et al., 1998). Analog model experiments suggest that rigid inclusions embedded in a homogeneous ductile matrix with coherent interfaces rotate during deformation under favourable conditions (Ghosh and Ramberg, 1976; Passchier and Simpson, 1986; Ildefonse et al., 1992; Arbaret et al., 1996). On the contrary, rigid inclusions in a heterogeneous system may not experience rotation even when there is a rotational component in the deformation (Stewart, 1997; Hickey and Bell, 1999). It thus appears that independent criteria are to be used to discriminate curved inclusion trails formed within rotating and non-rotating porphyroblasts (e.g. Passchier and Trouw, 1996; Bell et al., 1998; Chan and Crespi, 1999).

This review exclusively deals with inclusion trail structures developing in consequence to relative rotation of porphyroblasts growing over a pre-existing passive foliation during a single phase of deformation and metamorphism. With the advent of advanced PC software, numerical simulation of trail patterns within rotating porphyroblasts commenced as an area of major interest (Masuda and Mochizuki, 1989; Bjornerud and Zhang, 1994; Beam, 1996). Earlier studies along this line have revealed that relative rates of rotation and growth of porphyroblast are the principal parameters controlling the trail pattern (Mandal and Banerjee, 1987). Beam (1996) has further shown that porphyroblasts can grow by constant increments of radius, surface area and volume, each producing different trail patterns. Additional complexities in the trail pattern may also arise due to the deflection of foliation in consequence to heterogeneous strain induced by the porphyroblast in its vicinity. Based on the velocity field around a rigid sphere hosted in a viscous matrix with a coherent interface, different patterns of inclusion trails have been simulated numerically by varying the initial orientation of foliation markers (Masuda and Ando, 1988; Masuda and Mochizuki, 1989). It has been shown analytically that the degree of coupling between the porphyroblast and matrix influences the velocity field, and thereby controls the trail patterns (Bjornerud, 1989; Bjornerud and Zhang, 1994). All these models are two-dimensional and Gray and Busa (1994) advanced them to three dimensions.

The numerical models so far discussed deal with porphyroblasts of equant shape, which rotate with a constant angular velocity. The kinematic analysis reveals that non-spherical porphyroblasts rotate with changing angular velocity during progressive deformation. Beam (1996) has presented a kinematic model for the development of trail structures within non-spherical porphyroblasts under simple shear and a combination of simple shear and pure shear. His model, however, does not consider the effect of heterogeneous strain around the porphyroblast.

Jeffery's velocity functions, given in the earlier section can be applied to investigate the development of inclusion trails within synkinematic, rotating porphyroblasts of both equant and inequant shapes considering the heterogeneous flow of matrix around the porphyroblast (cf. Jezek et al., 1999; Mandal et al., 2000). The following factors appear to be effective in controlling the geometry of inclusion trails: (1) the initial orientation of foliation markers, (2) the ratio of pure shear and simple shear rates in the bulk deformation, (3) the ratio of the rates of rotation and growth of porphyroblast, and (4) the initial orientation and the ratio of growth rates along the axial directions of inequant porphyroblast.

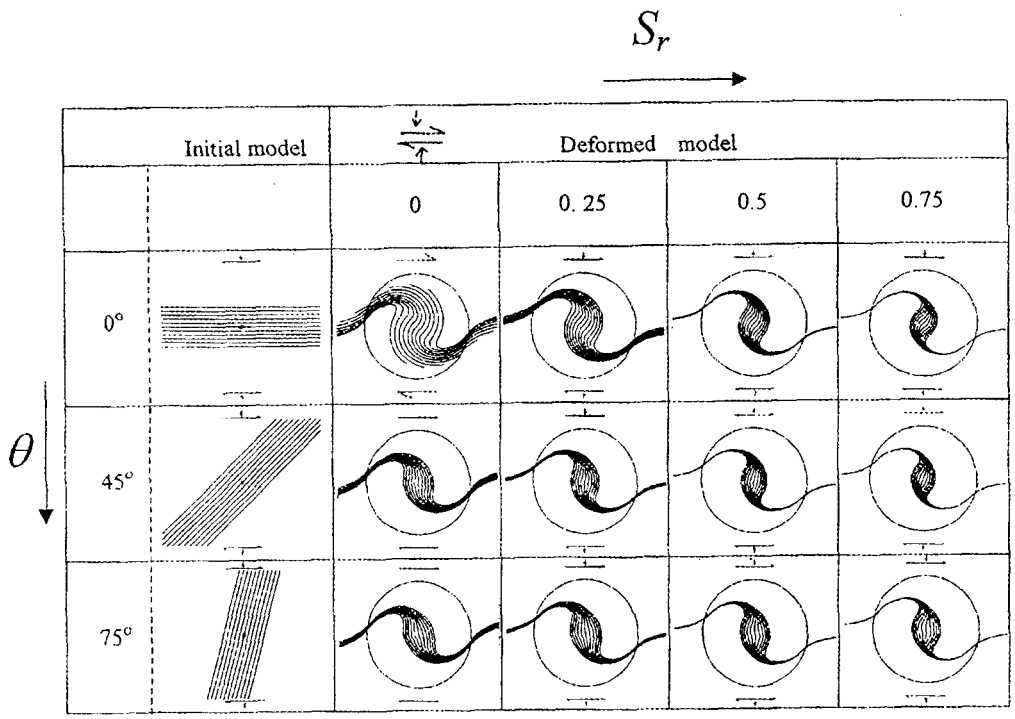

Fig. 21 Inclusion trail patterns in synkinematic porphyroblasts with θ less than 90°, where θ is the initial orientation of marker. S_r is the ratio of pure shear and simple shear rates. Note that, the central trails show reversal in curvatures for large values of S_r. Finite bulk shear in models was 5. Ratio of growth rates along axial directions = 1.

Trail patterns in equant porphyroblasts

Earlier workers (e.g, Masuda and Mochizuki, 1989) have shown that the trail patterns in radially growing equant porphyroblasts depend mainly on the initial orientation of marker foliation. Additional complexities in the trail patterns may arise if the effects of pure shear component in the bulk simple shear flow are taken into account. Porphyroblasts overgrowing markers initially inclined with the shear direction at angles between 0° and 90° do not show significant variation in the trail pattern with an increase in pure shear component in the bulk deformation (Fig. 21). The overall patterns are represented by sigmoidal curves, as commonly seen in natural porphyroblasts. The central trail (i.e. the trail passing through the center of the porphyroblast) consists of two segments symmetric about the center. The individual segments of the central trail do not generally show reversal in curvature, as revealed in earlier numerical models (Masuda and Mochizuki, 1989). However, when the marker is at a high angle with the shear direction and the ratio of pure shear and simple shear rates is large (> 0.5), they show reversal in curvature, giving rise to a sinuous pattern (Fig. 21). With decrease in the ratio of growth rate and rotation rate of porphyroblast, sigmoidal trail patterns are progressively replaced by spiral patterns (Fig. 22).

The influence of the strain ratio Sr on the trail patterns is most significant when the markers have negative inclination. For example, porphyroblasts, with markers initially at an angle of - 45°, show a systematic variation in the geometry of inclusion

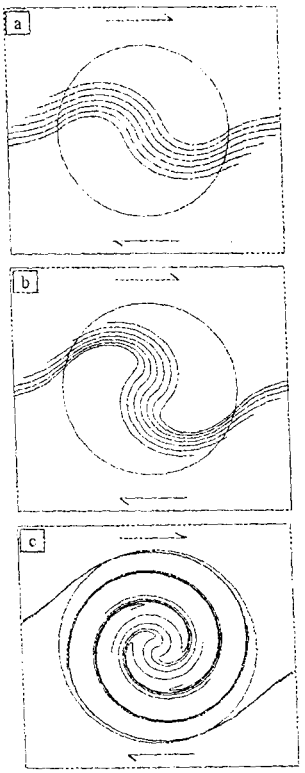

Fig. 22 Variations in trail patterns with increase in the ratio of rotation rate and growth rate of porphyroblast for $S_r = 0$. The ratios of rotation rate and growth rate of porphyroblast were 2.5, 5 and 25 radian/length in (a), (b) and (c) respectively. Marker foliation was parallel to the shear direction. Ratio of growth rates along axial directions = 1.

pattern, as the ratio of pure shear and simple shear rates in the bulk deformation is increased (Fig. 23). In simple shear ($S_r = 0$) the pattern is characterized by a central trail with sinuous segments astride the center, whereas the peripheral trails are typically convex outward (Fig. 23). With an increase in Sr value, peripheral trails tend to become convex inward resembling the 'millipede' structures described by Bell (1985). At larger values of S_r, the peripheral trails take the form of a hook-shaped fold, whereas the central trail assumes sigmoidal geometry. With further increase in Sr, the pattern turns into a simple one that consists of typical sigmoidal shaped trails. The spectrum of inclusion trail geometries arising from various combinations of Sr and negative inclinations of foliation is shown in Fig. 23.

Trail patterns in inequant porphyroblast

Trail patterns within inequant porphyroblasts can be simulated in simple shear and a combination of simple shear and pure shear by varying the initial orientations of the long axis of porphyroblast and the foliation marker, and the ratio of growth rates along the axial directions of porphyroblast. The diverse trail patterns obtained from these simulations can be classified into a number of types (Fig. 24). *Type 1* : The central trail is sinuous and confined by outward-convex peripheral trails. *Type 2* : The trails over the entire porphyroblast are sigmoidal in geometry. *Type 3* : The central trail is sigmoidal and is confined by inward-convex peripheral trails. *Type 3* trails can again be classified into four sub-types. *Type 3a* : The peripheral trails show a side stepping of their axial traces and the curvature of the trails progressively increases outward. *Type 3b* : The peripheral trails do not show side stepping and their curvature progressively decreases outward. *Type 3c* : The peripheral trails do not show side stepping and their curvature first decreases followed by an increase away from the center similar to those in 'millipede' structure. *Type 3d* : The central trail is much less curved than the other types and the curvature of the trails progressively increases outward. *Type 4* : In this pattern peripheral trails are convex outward. The pattern can be further subdivided into two types: *Type 4a* - the central trail is more or less straight and confined by trails with increasing outward convexity, and *Type 4b* - the central trail has two sinuous segments. *Type 5* : The peripheral trails are convex inward. Depending upon the pattern of the central trail, the type can again be subdivided into three sub-types. *Type 5a* : The central trail has two sinuous segments. *Type 5b* : The central trail with a step-like geometry. *Type 5c* : a combination of *types 5a* and *5b*. The kinematic and geometrical condi-

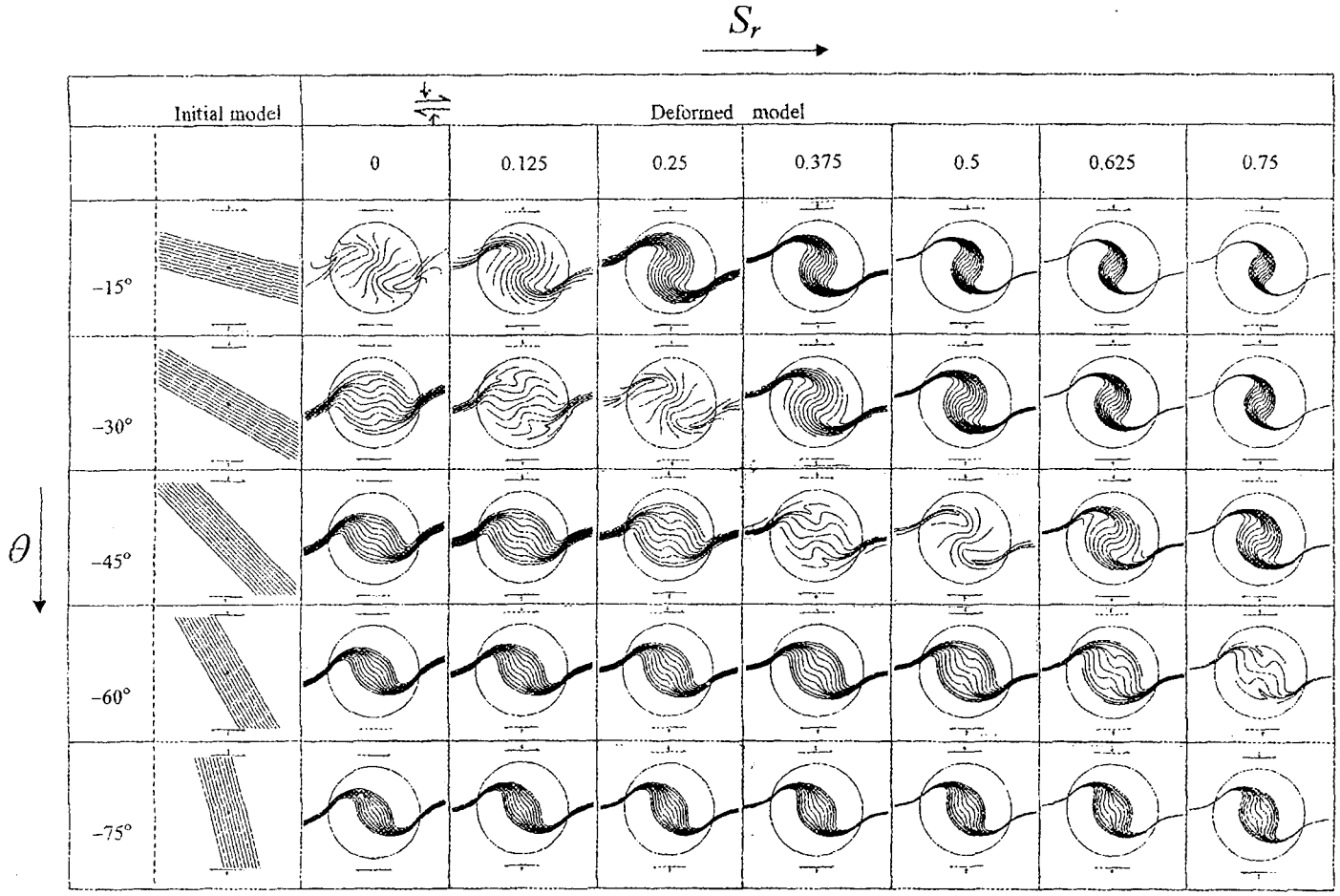

Fig. 23 A map of different trail patterns of porphyroblasts in θ (< 0) versus S_r space. Finite bulk shear in the models was 5. Ratio of growth rates along axial directions = 1.

Table 3 :

The geometrical and kinematic conditions for the development of different types of trail patterns in non-spherical porphyroblasts. The numbers in Italics refer to the types of trail structures as stated in the text.

Simple Shear
($S_r = 0$)

Combination of Simple Shear and Pure Shear
($S_r = 0.25$)

θ = 85°

G_r \ φ	-45°	0°	45°	85°
1.5	*1*	*1*	*1*	*4b*
3	*3a*	*1*	*2*	*4a*

G_r \ φ	-45°	0°	45°	85°
1.5	*1*	*1*	*1b*	*1*
3	*3b*	*1*	*1*	*4a*

θ = 45°

G_r \ φ	-45°	0°	45°	85°
1.5	*3b*	*2*	*2*	*2*
3	*3b*	*1*	*4a*	*2*

G_r \ φ	-45°	0°	45°	85°
1.5	*3b*	*4a*	*4a*	*1*
3	*3b*	*1*	*4a*	*1*

θ = 0°

G_r \ φ	-45°	0°	45°	85°
1.5	*3b*	*1*	*3a*	*3a*
3	*3c*	*2*	*4c*	*3c*

G_r \ φ	-45°	0°	45°	85°
1.5	*3b*	*2*	*1*	*1*
3	*3b*	*4a*	*3b*	*3c*

θ = -10°

G_r \ φ	-45°	0°	45°	85°
1.5	*3a*	*3a*	*3a*	*3a*
3	*3c*	*5b*	*3d*	*3d*

G_r \ φ	-45°	0°	45°	85°
1.5	*3b*	*2*	*3a*	*3a*
3	*3b*	*2*	*3a*	*3c*

θ = -45°

G_r \ φ	-45°	0°	45°	85°
1.5	*4b*	*1*	*1*	*1*
3	*5a*	*1*	*3b*	*2*

G_r \ φ	-45°	0°	45°	85°
1.5	*5b*	*3a*	*5b*	*5b*
3	*5c*	*3a*	*5b*	*5c*

θ = Initial inclination of marker with the shear direction,
ϕ = Initial inclination of a-axis of porphyroblast,
G_r = Ratio of growth rates along the axial directions of porphyroblast,
S_r = Ratio of pure shear and simple shear rates in bulk deformation.

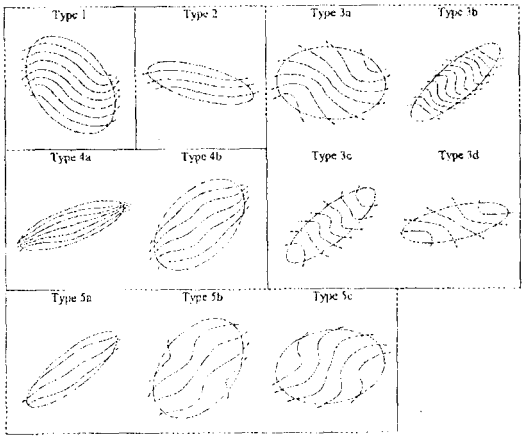

Fig. 24 Types of trail structures in elongate porphyroblasts, obtained from numerical model experiments. Ratio of growth rates along axial directions ranges between 1.5 and 3.

tions for the development of these different types of trail structures are summarized in Table -3.

ACKNOWLEDGEMENTS

We wish to thank Professors C. Passchier, C. Simpson and D. G. De Paor for their critical comments on our work dealing with mantle structures around inequant porphyroclasts. We also thank Professor D. Mukhopadhyay for his suggestions to improve the manuscript. The present work was carried out under a project of Department of Science and Technology (India), sanctioned to N. M. S. K. S is grateful to the University Grant Commissions, India for the Research Fellowship. C. C acknowledges the infrastructural facilities provided by the Indian Statistical Institute, Calcutta.

REFERENCES

Arbaret L, Diot A and Bouchez J L, 1996. Shape fabrics of particles in low concentration suspensions: 2D analogue experiments and application to tiling in magma. *Jour Struct Geol*, 18, 941-950.

Beam E C, 1996. Modeling growth and rotation of porphyroblasts and inclusion trails. In: De Paor, D.G (Ed), Structural Geology and Personal Computers. Computer Methods in the Geosciences 15, 247-258. *Pergamon Press, London.*

Bell T H, 1985. Deformation partitioning and porphyroblast rotation in metamorphic rocks: a radical reinterpretation. *Jour Meta Geol*, 3, 109-118.

Bell T H, Forde A and Hayward N, 1992b. Do Smoothly curving, spiral-shaped inclusion trails signify porphyroblast rotation? *Geology*, 20, 59-62.

Bell T H and Hickey K A, 1997. Distribution of pre-folding linear indicators of movement direction around the Spring Hill Synform, Vermont: significance for mechanism of folding in this portion of the Appalachians. *Tectonophys*, 274, 275-294.

Bell T H, Hickey K A and Upton G J G, 1998. Distinguishing and correlating multiple phases of metamorphism across a multiply deformed region using the axes of spiral, staircase and sigmoidal inclusion trails in garnet. *Jour Meta Geol*, 16, 767-794.

Bell T H and Johnson S E, 1989. Porphyroblast inclusion trails: the key to orogenesis. *Jour Meta Geol*, 7, 279-310.

Bell T H, Johnson S E, Davis B, Forde A, Hayward, N and Wilkins C, 1992a. Porphyroblast inclusion-trail orientation data: eppure non son girate! *Jour Meta Geol*, 10, 295-307.

Bell T H and Rubenach M J, 1980. Crenulation cleavage development - evidence for progressive, bulk inhomogeneous shortening from "millipede" microstructures in the Robertson River Metamorphics. *Tectonophys*, 68, T9-T15.

Bjornerud M G, 1989a. Mathematical model for folding of layering near rigid objects in shear deformation. *Jour Struct Geol*, 11, 245-254.

Bjornerud M G, 1989b. Toward a unified conceptual framework for shear-sense indicators. *Jour Struct Geol*, 11, 1045-1049.

Bjornerud MG and Zhang H, 1994. Rotation of porphyroblasts in non-coaxial deformation: insights from computer simulations. *Jour Meta Geol*, 12, 135 - 139.

Bjornerud M G and Zhang H, 1995. Flow mixing object matrix coherent mantle growth and the development of porphyroclast tails *Jour Struct Geol* 17, 1347-1350.

Chan Y-C and Crespi J M, 1999. Albite porphyroblasts with sigmoidal inclusion trails and their kinematic implications: an example from the Taconic Allochthon, west-central Vermont. *Jour Struct Geol*, 21, 1407-1417.

Choukroune P, Gapais D and Merle O, 1987. Shear criteria and structural symmetry. *Jour Struct Geol*, 9, 525-530.

Cox H L, 1952. The elasticity and strength of paper and other fibrous materials. *British Jour Appl Phys*, 3, 72-79.

Einstein A, 1911. Eine neue Bestimmung der Molekuldimensionen. *Ann. D. Physik* 34, 591.

Eshelby J D, 1957. The determination of the elastic field of an ellipsoidal inclusion, related problems. *Proc Roy Soc Lond.*, A241, 376-396.

Eshelby J D, 1959. The elastic field outside an ellipsoidal inclusion. *Proc Roy Soc Lond.*, A252, 561-569.

Ferguson C C, 1979. Rotations of elongate rigid particles in slow non-Newtonian flows. *Tectonophys*, 60, 247 - 262.

Gay N C, 1968. Pure shear and simple shear deformation of inhomogeneous viscous fluids. 1. *Theory. Tectonophys*, 5(3), 211-234.

Ghosh S K, 1975. Distortion of planar structures around rigid spherical bodies. *Tectonophys*, 28, 185-208.

Ghosh S K and Ramberg H, 1976. Reorientation of inclusions by combination of pure shear and simple shear. *Tectonophys*, 34, 1-70.

Ghosh S K and Ramberg H, 1978. Reversal of spiral direction of inclusion-trials in paratectonic pophyroblast. *Tectonophys*, 52, 83-97.

Ghosh S K and Sengupta S, 1973. Compression and simple shear test models with rigid and deformable inclusions. *Tectonophys*, 17, 133-175.

Gray N H and Busa M D, 1994. The three-dimensional geometry of simulated porphyroblast inclusion trails: inert marker, viscous-flow models. *Jour Meta Geol*, 12, 575-587.

Hanmer S and Passchier C W, 1991. Shear sense indicators: a review. Geol Surv Cand Paper 90, 1-71.

Hickey K A and Bell T H, 1999. Behaviour of rigid objects during deformation and metamorphism: a test using schists from the Bolton syncline, Connecticut, USA. Jour Meta Geol, 17, 211-228.

Hooper R J and Hatcher R D, 1988. Mylonites from the Towaliga fault zone, central Georgia: products of heterogeneous non-coaxial deformation, Tectonophys, 152, 1-17.

Ildefonse B and Mancktelow N S, 1993. Deformation around rigid particle: influence of slip at the particle/matrix interface. Tectonophys, 221, 345-359.

Ildefonse B, Sokoutis D and Mancktelow N S, 1992. Mechanical interactions between rigid particles in a deforming ductile matrix. Analogue experiments in simple shear flow. Jour Struct Geol, 14, 1253-1266.

Jeffery G B, 1922. The motion of ellipsoidal particles immersed in a viscous fluid. Proceedings of the Royal Society of London A (120), 161-179.

Jezek J, Saic S, Segeth K and Schulmann K, 1999. Three-dimensional hydrodynamical modelling of viscous flow around a rotating ellipsoidal inclusion. Comp & Geosc, 25, 547-558.

Ji S, Zhao P and Saruwatari K, 1997. Fracturing of garnet crystals in anisotropic rocks during uplift. Jour Struct Geol 19, 603-620.

Johnson S E and Bell T H, 1996. How useful are 'millipede' and other similar porphyroblast microstructures for determining synmetamorphic deformation histories? Jour Meta Geol, 14, 15-28.

Johnson S E and Moore R R, 1996. De-bugging the "millipede" porphyroblast microstructure: a serial thin-section study and 3-D computer animation. Jour Meta Geol, 14, 3-14.

Lamb H, 1932. Hydrodynamics. Cambridge University Press, Cambridge, 738 pp.

Mandal N and Banerjee S, 1987. Rotation rate versus growth rate of syntectonic porphyroblasts: the controlling parameter of the shape of the inclusion trail. Tectonophys, 136, 165-169.

Mandal N and Chakraborty C, 1990. Strain fields and foliation trajectories around pre-, syn- and post-tectonic plutons in coaxially deformed terrains. Geol Jour, 25, 19-33.

Mandal N, Samanta S K and Chakraborty C, 2000. Development of mantle structures around elongate porphyroclasts: insights from numerical models. Jour Struct Geol, 22, 993-1008.

Masuda T and Ando S, 1988. Viscous flow around a rigid spherical body: a hydrodynamical approach. Tectonophys, 148, 337-346.

Masuda T and Mizuno N, 1996a. Deflection of non-Newtonian simple shear flow around a rigid cylindrical body by the finite element method. Jour Struct Geol 18, 1089-1100.

Masuda T and Mizuno N, 1996b. Computer modeling mantled porphyroclasts in Newtonian and no -

Newtonian simple shear viscous flows. Jour Struct Geol, 18, 1487-1491.

Masuda T and Mochizuki S, 1989. Development of snowball structures: numerical simulation of inclusion trails during synkinematic porphyroblast growth in metamorphic rocks. Tectonophys, 170, 141-150.

Mawer C K, 1987. Shear criteria in the Greenville Province, Ontario, Cand. Jour Struct Geol, 9, 531-539.

Muskhelishvilli N I, 1953. Some basic problems of the mathematical theory of elasticity. P. Noordhoff Ltd., Groningen-Holland, 704 pp.

Oertel G, 1965. Slow viscous flow of an incompressible suspension. Jour Eng and Mech Div, ASCE 91, 145-154.

Passchier C W, 1987. Stable positions of rigid objects in non-coaxial flow: a study in vorticity analysis. Jour Struct Geol, 9, 679-690.

Passchier C W, 1994. Mixing in flow perturbations: a model for development of mantle porphyroclasts in mylonites. Jour Struct Geol, 16, 733-736.

Passchier C W and Simpson C, 1986. Porphyroclast systems as kinematic indicators. Jour Struct Geol, 8, 831-844.

Passchier C W and Sokoutis D, 1993. Experimental modeling of mantled porphyroclasts. Jour Struct Geol, 15, 895-910.

Passchier C W and Speek P J H R, 1994. The kinematic interpretation of obliquely-transected porphyroblasts: an example from the Trois Seigneurs Massif, France. Jour Struct Geol, 16, 971-984.

Passchier C W, ten Brink C E, Bons P D and Sokoutis D, 1993. (objects as a gauge for stress sensitivity of strain rate in mylonites. Earth Planet Sc Lett, 120, 239-245.

Passchier C W and Trouw R A J, 1996. Microtectonics. Springer. 289 pp.

Passchier C W, Trouw R A J, Zwart H J and Vissers R L M, 1992. Porphyroblast rotation: eppur si move? Jour Meta Geol, 10, 283-294.

Pennacchioni G P, Fasolo L, Cecchi M M and Salasnich L, 2000. Finite-element modelling of simple shear flow in Newtonian and non-Newtonian fluids around circular rigid particle. Jour Struct Geol, 22, 683-692.

Powell C Mc A and Vernon R H, 1979. Growth and rotation history of garnet porphyroblasts with inclusion spirals in Karakoram Schist. Tectonophys, 54, 25-43.

Ramberg H, 1975. Particle paths, displacement and progressive strain applicable to rocks. Tectonophys, 28, 1-37.

Ramsay J G and Huber M I, 1987. The Techniques of Modern Structural Geology. Volume 2: Folds and Fractures. Academic Press, London.

Rast N, 1958. Metamorphic history of the Schichallion complex. Trans Roy Soc Edinburgh, 63(2), 413 - 432.

Rosenfeld J L, 1970. Rotated garnets in metamorphic rocks. Special Paper, Geological Society of America, 129 pp.

Schoneveld C, 1977. A study of some typical inclusion patterns in strongly paracrystalline rotated garnets. Tectonophys, 39, 453-471.

Simpson C and De Paor D, 1993. Strain and kinematic analyses in general shear zones. Jour Struct Geol, 15, 1-20.

Spry A, 1969. Metamorphic Textures. Pergamon Press, Oxford.

Stewart L K, 1997. Experimental investigation of the effects of fluid heterogeneity upon the motion of rigid ellipsoidal inclusions during bulk inhomogeneous shortening. Jour Struct Geol, 19, 1231-1243.

Stromgard K E, 1973. Stress distribution during deformation of boudinage and pressure shadows. Tectonophys, 16, 215-248.

ten Brink C E Bons P D and Passchier C W, 1993. Approximate stream functions for flow around rigid objects in shear zones. Abstract supplement No. 2 to terra Nova, 5-35.

ten Brink C and Passchier C W, 1995. Modeling of mantled porphyroclasts using non-Newtonian rock analogue materials. Jour Struct Geol, 17, 131-146.

Turcotte D and Schubert G, 1982. Geodynamics: Applications of Continuum Physics to Geological Problems. John Wiley and Sons, New York.

Van Der Driessche J and Brun J P, 1987. Rolling structures at large shear strain. Jour Struct Geol, 9, 691-704.

Wakiya S, 1956. Effect of a submerged object on a slow viscous flow: 2. A sphere in the flow between two parallel planes. Res Report of Facul Eng, Nugata University, 5, 1-12. (in Japanese)

Zwart H J, 1960. Relations between folding and metamorphism in the central Pyrenees. Geological Minjbouw 39d, 163.